BRNO UNIVERSITY OF TECHNOLOGY

VYSOKÉ UČENÍ TECHNICKÉ V BRNĚ

FACULTY OF MECHANICAL ENGINEERING

FAKULTA STROJNÍHO INŽENÝRSTVÍ

INSTITUTE OF PHYSICAL ENGINEERING

ÚSTAV FYZIKÁLNÍHO INŽENÝRSTVÍ

OPTIMIZING EXPERIMENTAL PARAMETERS FOR LIBS ANALYSIS OF HARD TISSUES

OPTIMALIZACE EXPERIMENTÁLNÍCH PARAMETRŮ PŘI ANALÝZE TVRDÝCH TKÁNÍ METODOU LIBS

MASTER'S THESIS

DIPLOMOVÁ PRÁCE

AUTHOR
AUTOR PRÁCE
Bc. Aida Fazlić

VEDOUCÍ PRÁCE
SUPERVISOR
doc. Ing. Pavel Pořízka, Ph.D.

BRNO 2023

VYSOKÉ UČENÍ TECHNICKÉ V BRNĚ FAKULTA STROJNÍHO INŽENÝRSTVÍ

Assignment Master's Thesis

Institut:	Institute of Physical Engineering
Student:	**Bc. Aida Fazlić**
Degree programm:	Precise Mechanics and Optics
Branch:	no specialisation
Supervisor:	**doc. Ing. Pavel Pořízka, Ph.D**
Academic year:	2022/23

As provided for by the Act No. 111/98 Coll. on higher education institutions and the BUT Study and Examination Regulations, the director of the Institute hereby assigns the following topic of Master's Thesis:

Optimizing experimental parameters for LIBS analysis of hard tissues

Brief Description:

Laser-induced breakdown spectroscopy (LIBS) allows the detection of minor and trace elements with high spatial resolution and high repetition rate. As a result, LIBS has become a useful tool in hard tissue analysis and is gaining popularity in medical and clinical research. From the physical principle of the method, it is clear that an increase in analytical performance can be achieved by two approaches (or a combination of both) 1) increasing the ablated mass of the sample; 2) increasing the plasma temperature. In the first case, however, the ablation crater is enlarged and, as a consequence, the spatial resolution of the method is degraded. One method that allows to increase the analytical performance while maintaining high spatial resolution is an experimental setup using two time-resolved laser pulses (DP-LIBS). However, to achieve maximum analytical performance, it is necessary to optimize the experimental parameters with respect to the sensitivity to the selected analytes while maintaining the spatial resolution (size of the ablation crater). Therefore, an appropriate combination of experimental parameters (e.g., laser energy and wavelength) needs to be selected. In particular, this work will focus on the study of multi-pulse LIBS method in the detection of heavy metals and other analytes in hard tissue matrix (teeth and bones of model animals).

Master's Thesis goals:

I. Literature research of current state of the art in the field of hard tissues analysis by LIBS method
II. Selection of reference samples and optimization of experimental parameters with regards to lateral resolution and sensitivity
III. Comparison of various wavelengths and other parameters of multi-pulse LIBS to improve the analytical performance, sensitivity versus lateral resolution
IV. Detection of selected heavy metals and other analytes in hard tissues, estimating the limits of detection

Recommended bibliography

HAHN, David W. and Nicoló OMENETTO. Laser-Induced Breakdown Spectroscopy (LIBS), Part II: Review of Instrumental and Methodological Approaches to Material Analysis and Applications to Different Fields. Applied Spectroscopy. 2012, 66(4), 347-419. ISSN 0003-7028. doi:10.1366/11- 06574

LIMBECK, A., L. BRUNNBAUER, H. LOHNINGER, et al. Methodology and applications of elemental mapping by laser-induced breakdown spectroscopy: Review of Instrumental and Methodological Approaches to Material Analysis and Applications to Different Fields. Analytica Chimica Acta. 2021, 1147(4), 72-98. ISSN 00032670. Dostupné z: doi:10.1016/j.aca.2020.12.054

PROCHAZKA, David, Pavel POŘÍZKA, Jan NOVOTNÝ, et al. Triple-pulse LIBS: laser-induced breakdown spectroscopy signal enhancement by combination of pre-ablation and re-heating laser pulses. Journal of Analytical Atomic Spectrometry. 2020, 35(2), 293-300. ISSN 0267-9477. Dostupné z: doi:10.1039/C9JA00323A

Deadline for submission Master's Thesis is given by the Schedule of the Academic year 2022/23.

In Brno,

L. S.

prof. RNDr. Tomáš Šikola,CSc.	doc. Ing. Jiří Hlinka, Ph.D.
Director of the Institute	FME dean

Abstract

This diploma thesis focused on the detection and analysis of heavy metals, particularly lead (Pb), in hard tissues using hydroxyapatite standards and laser-induced breakdown Spectroscopy (LIBS) instrumentation. The study utilized various laser wavelengths of 1064 nm, 532 nm, and 266 nm, as well as different laser configurations, including single-pulse (SP) LIBS and double-pulse (DP) LIBS in both orthogonal and collinear arrangements. The optimization of laser parameters such as wavelength, defocus, gate delay, interpulse delay, and energy was performed, with the signal-to-background ratio (SBR), limit of detection (LOD), and resolution corresponding to the diameter of the ablation crater serving as the basic parameters for determining the optimal combination of parameters. The findings of this study provide important insights into the optimal LIBS parameters for the detection and analysis of heavy metals in hard tissues, which can potentially have significant implications for medical research.

Abstrakt

Tato diplomová práce se zaměřuje na detekci a analýzu těžkých kovů, zejména olova (Pb), v tvrdých tkáních pomocí hydroxyapatitových standardů a spektroskopie laserem buzeného plazmatu (LIBS). Studie využívala různé vlnové délky laseru 1064 nm, 532 nm a 266 nm, stejně jako různé konfigurace laseru, včetně jednopulzní (SP, z angl. single-pulse) LIBS a dvojpulzní (DP, z angl. double-pulse) LIBS v ortogonálním a kolineárním uspořádání. Byla provedena optimalizace parametrů laseru, jako jsou vlnová délka, defokus, doba zpoždění, mezipulzní doba zpoždění a energie. Poměr signál-ke-šumu (SBR), limit detekce a rozlišení odpovídající průměru ablačního kráteru sloužily jako základní parametry pro určení optimální kombinace parametrů. Výsledky této studie poskytují důležité poznatky o optimálních parametrech LIBS pro detekci a analýzu těžkých kovů v tvrdých tkáních, což může mít potenciálně významné dopady pro lékařský výzkum.

Keywords

laser-induced breakdown spectroscopy (LIBS), single-pulse LIBS, double-pulse LIBS, heavy metals, hard tissues, orthogonal, collinear, gate delay, defocus, energy, interpulse delay, signal to background ratio, limit of detection, ablation crater

Klíčová slova

spektroskopie laserem buzeného plazmatu (LIBS), single-pulse LIBS, double-pulse LIBS, těžké kovy, tvrdé tkáně, ortogonální, kolineární, doba zpoždění, defokus, energie, mezipulzní doba zpoždění, poměr signál-šum, limit detekce, ablační kráter

Bibliographic citation

FAZLIĆ, Aida. *Optimalizace experimentálních parametrů při analýze tvrdých tkání metodou LIBS* [online]. Brno, 2023 [cit. 2023-05-04]. Dostupné z: https://www.vut.cz/studenti/zav-prace/detail/145639. Diplomová práce. Vysoké učení technické v Brně, Fakulta strojního inženýrství, Ústav fyzikálního inženýrství. Vedoucí práce Pavel Pořízka.

Author's Declaration

I declare that I have independently written this thesis and that I have correctly and fully cited all literary sources used. The thesis is the property of the Faculty of Mechanical Engineering, Brno University of Technology, in terms of its content and may only be used for commercial purposes with the consent of the thesis supervisor and the dean of the Faculty of Mechanical Engineering, Brno University of Technology.

May 10th, 2023 .....

Bc. Aida Fazlić

Acknowledgment

I would like to express my sincere gratitude to Ministerstvo školství, mládeže a tělovýchovy (Ministry of Education, Youth and Sports) for providing me with a scholarship throughout my studies, which made my stay in the Czech Republic possible. I am also grateful to Prof. Dipl.-Ing. Dr.techn. Andreas Limbeck and Ing. Birgit Achleitner, who provided me with the basic knowledge of LIBS during my Erasmus stay at TU Wien and made it a productive and comfortable experience. I would like to extend my thanks to doc. Ing. Pavel Pořízka, Ph.D., who not only supervised my thesis but also provided me with numerous opportunities and made my Erasmus stay possible. Lastly, I would like to thank Ing. Anna Konečná and Ing. Jakub Buday for their invaluable advice, corrections, and patience throughout the entire process of measuring and writing the thesis.

Content

1 Introduction

Laser technology has played a critical role in the advancement of elemental and spectroscopic analysis. Spectroscopy is a valuable experimental technique used to study the interaction between matter and electromagnetic radiation. It is based on the principle that every atom and molecule has the ability to absorb or emit electromagnetic waves with different wavelengths. This thesis focuses on laser-induced breakdown spectroscopy (LIBS). This technique enables multi-elemental analysis of materials and has gained popularity due to its minimal sample preparation requirement, ability to analyze solids, liquids, aerosols, and gases, and real-time analysis capability. The thesis's focus is on optimizing the experimental parameters for LIBS detection of heavy metals in hard tissues, such as laser energy and gate delay. The thesis also explains other essential parameters and how they affect LIBS measurements, and compares three different laser wavelengths, optimizing the parameters using hydroxyapatite standards. To address ethical considerations and the difficulty of obtaining bone samples, hydroxyapatite samples were utilized as a suitable alternative in this study.

LIBS has found numerous applications in different fields, including medical biology, industry, archaeology, chemistry, and space exploration. In recent years, LIBS has emerged as a powerful tool for various medical applications, including the detection of cancer cells and bacteria. However, the scope of this thesis is centered on the critical detection of heavy metals in organisms. Heavy metals, such as lead and cadmium, can pose severe health risks when present in certain quantities. It is therefore of utmost importance to detect and quantify these toxic elements in a timely manner. LIBS, through the emission of characteristic spectral lines, not only enables the detection of heavy metals in the body but also allows for their accurate quantification. This research aims to explore the potential of LIBS as a reliable method for the detection of heavy metals in organisms, thereby contributing to the field of medical diagnostics and environmental monitoring.

LIBS, despite its numerous advantages, is not without limitations, particularly regarding its sensitivity. One of the challenges faced in LIBS is to improve the lateral resolution without compromising the high signal intensities necessary for accurate detection. To address this issue, various enhancement methods have been proposed, including the atmosphere control method and the spatial constraint method. These techniques aim to optimize the laser-induced plasma conditions and enhance the emission signals. However, in the context of this thesis, the focus was on the application of the multiple-pulse enhancement method.

Both single-pulse (SP) and multiple-pulse LIBS techniques, including double-pulse (DP) LIBS with collinear and orthogonal configurations, have been explored for their potential to improve the detection of heavy metals in hard tissues. The present thesis focuses on the comparative analysis of SP and DP-LIBS methods using different laser wavelengths, defocus, energies, gate delays, and interpulse delays. The main objective was to enhance the analytical performance, sensitivity versus lateral resolution, and lower limit of detection (LOD) for heavy metal detection in hard tissues. Overall, this thesis aims to contribute to the development of more effective and efficient LIBS-based techniques for detecting heavy metals in hard tissues.

This thesis is organized into four main parts. The first part (Chapter 2) provides a theoretical introduction to spectroscopy and the underlying physics principles. It also includes an explanation of the LIBS technique, its instrumentation, and the physics behind it. Additionally, this chapter covers information about heavy metals and hard tissues.

Chapter 3 presents an overview of the current state of knowledge in the field. This includes a review of previously conducted experiments and published articles focused on optimizing parameters for different laser wavelengths by LIBS and analyzing heavy metals in hard tissues. Chapter 4 describes the experimental setup used in this thesis, including details about the sample preparation, laser system, and data acquisition. Finally, Chapter 5 presents the results obtained from the conducted experiments and discusses the achievement of the set goals. The results are analyzed and interpreted to evaluate the analytical performance, sensitivity, and limit of detection of the developed LIBS-based methodology for heavy metals detection in hard tissues.

2 Theory

2.1 Spectroscopy

“For the rest of my life I will reflect on what light is“ are the words of Albert Einstein. Light is, indeed, a topic that was interesting for scientists throughout the centuries and is still the subject of many researchers. It can behave as both a particle and a wave. Spectroscopy is the branch of physics that studies electromagnetic radiation, and light is the result of this radiation. More specifically, this branch of science studies how electromagnetic radiation interacts with matter. To better understand this topic, the first thing we should know is the explanation of the term "wave". In physics, a wave is described as a disturbance propagating from one place to another, described by parameters such as frequency, phase, direction, speed, and wavelength. Light is an electromagnetic wave, which can be described as rapid, periodic changes in space and time of electric and magnetic fields. The electric and magnetic fields are perpendicular to each other and perpendicular to the direction of the waves [1]. The properties of these fields can be described using Maxwell's equations. The electromagnetic spectrum represents different categories of electromagnetic radiation that share similar properties. Each category has a characteristic range of corresponding frequencies and wavelengths, as it is shown in Figure 1.

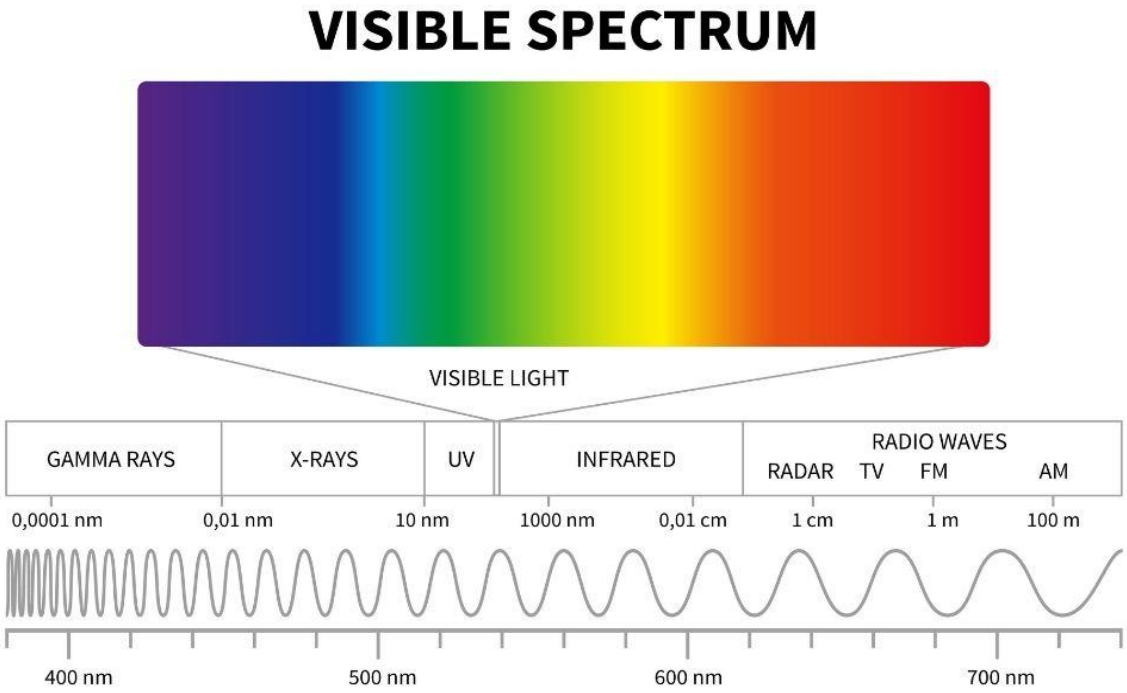

Figure 1: Electromagnetic spectrum [2].

Studying electromagnetic patterns using spectroscopy methods can reveal details about the composition and structure of a substance. There are two types of patterns: continuous and discrete. Discrete patterns can be either from emitting or absorbing light. Every element can absorb certain wavelengths of light. Joseph von Fraunhofer discovered more than 550 absorption lines, which was a significant contribution to the field of spectroscopy. Absorption occurs when the energy of an electromagnetic wave is transferred to electrons, causing them to move from a lower energy level to a higher one [3].

Emission is the process that is opposite to absorption and can occur in two ways: spontaneous and stimulated. When an electron in an excited state interacts with an incident photon, it can undergo stimulated emission, transitioning back to the ground state and releasing energy in the form of two photons. This is different from spontaneous emission, where energy is naturally released. Stimulated emission results in the emission of two identical photons, which propagate in a single direction and possess the same frequency and energy. The rate of stimulated emission is much faster than spontaneous emission, and it is dependent on the intensity of the incident light and the number of electrons occupying the excited state. Laser light, which is monochromatic, is produced by stimulated emission [4].

The classification of spectroscopy is usually made based on the type of radiant energy (electromagnetic radiation, acoustic radiation, etc.), and the type of interaction between the energy and matter (absorption, emission, fluorescence). Spectroscopy can also be divided into atomic spectroscopy and molecular spectroscopy. This work focuses on electromagnetic atomic emission spectroscopy [4].

2.2 Laser-induced breakdown spectroscopy - LIBS

After the invention of high-intensity laser sources, new possibilities for elemental analysis were opened. One of them is laser-induced breakdown spectroscopy (LIBS). Inductively Coupled Plasma Optical Emission Spectroscopy (ICP-OES) is, next to LIBS, one of the most widespread emission spectroscopic techniques. Some other emission spectroscopic techniques include X-ray Fluorescence Spectroscopy (XRF), Raman Spectroscopy, and Chemiluminescence Spectroscopy [5].

LIBS allows multi-elemental analysis of all types of materials. The development of this real-time technique was possible mainly thanks to the technological progress that is constantly taking place in the field of spectrometers, detectors, and lasers. A high-intensity laser source is used to excite part of the sample, whereupon the plasma is induced. The detection of emission spectra then allows the determination of the concentration of the elements present in the plasma plume, therefore in the sample [5].

LIBS operates by generating a plasma plume through a laser-matter interaction, exciting atoms and ions that release photons of specific energy when transitioning to a lower energy level, with the emitted light being collected and captured by lenses and detectors to determine the elements present in the sample based on their unique spectral lines [6].

LIBS technique allows for both qualitative and quantitative analysis of samples. Quantitative analysis is focused on determining the precise quantities or concentrations of those elements within the sample, while qualitative analysis can identify expected or unknown elements present in a sample. Detecting certain elements such as chlorine may sometimes require signal enhancement techniques. In quantitative analysis, a reference matrix with known concentrations of the element of interest is prepared and used to compare the relative signal intensities of standard and real samples. The resulting calibration curve displays the relationship between signal intensity (arb. u.) and element concentration (ppm - parts per million) [5].

There is almost no sample preparation required, which is also one of the main advantages of LIBS. In the realm of analytical chemistry, LIBS is recognized as a semi-destructive analytical technique because it only removes a small portion of the sample during the analysis process. Despite its partial destructiveness, this method is considered cost-effective, as it allows for depth profiling, a process of examining the elemental

composition of a sample at varying depths, providing valuable insights into the distribution of elements within the sample. In order to perform depth profiling, a laser is used to ablate the surface of the sample repeatedly, with the resulting plasma plume emission spectra being analyzed to determine the elemental composition at various depths [7]. LIBS has the capability to detect the majority of elements present in the periodic table. It can also be combined with other spectroscopic methods to create tandem LIBS, which enables simultaneous detection of multiple elements. However, it is not a perfect technique and requires optimization to be considered a standardless method. Various factors, including the surrounding atmosphere, laser pulse wavelength, and pulse length, can affect the accuracy of the results. Efforts are being made to improve the technique's detection limit (LOD), which refers to the lowest concentration of an element that can be reliably detected [5].

Matrix effects refer to the influence of a sample's chemical and physical properties on the signal intensity measured during analysis. These effects may make it challenging to detect specific elements due to interference from emission lines of other elements and can also impact the accuracy of quantitative analysis through physical matrix effects. Physical matrix effects are influenced by a range of factors, such as the sample's physical structure, thermal properties, surface roughness, and density. The crystallographic structure of the sample, including face-centered cubic (FCC) and hexagonal close-packed (HCP) structures, can also impact matrix effects. In addition to these factors, the thermal conductivity and specific heat capacity of the sample can influence the formation of plasma and light emission during analysis. Lastly, surface roughness and density can affect the depth of laser penetration and the subsequent formation of plasma [8].

LIBS is still considered one of the most effective techniques for elemental analysis, with widespread use across multiple fields. For instance, this method is often employed in environmental monitoring to detect toxic elements and assess soil quality. Additionally, it has applications in space research, with a growing use in analyzing samples from Mars. In the industrial sector, LIBS is utilized for the quality control of semiconductors. Moreover, in biomedical research, LIBS is employed to identify bacteria, spores, and toxic elements in tissues that could potentially cause diseases such as cancer. Going forward, the goal is to further develop this technique as a tool for surgical operations [9].

2.2.1 Sample ablation and formation of plasma

For LIBS technology to be successful, an understanding of the physical and chemical properties of laser-induced plasmas is necessary. Plasma is usually defined as an ionized gas. The minimum temperature at which plasma can form varies depending on several factors, such as the specific type of plasma and the techniques employed to generate it. Till this day it still remains a very complex and intensively studied subject [10].

A small amount of sample is vaporized by a laser pulse to create a plasma plume consisting of highly excited atoms and ions emitting light at characteristic wavelengths. The plasma plume rapidly expands and cools down, and its characteristics such as temperature, density, and chemical composition depend on several factors including laser energy, pulse duration, and sample properties. The formation of shock waves within the plasma plume is a crucial aspect of plasma plume physics, with shock waves being generated due to the rapid expansion of the plasma, leading to significant effects on the plasma plume characteristics. These shock waves can cause a rapid drop in the plasma temperature, affecting the emission spectra of the plasma, and induce turbulence that can affect the transport of atoms and ions within the plasma plume. The surrounding atmosphere can also have a significant influence

on the plasma plume, affecting the cooling rate, plasma temperature, density, and transport of atoms and ions, leading to changes in the chemical composition of the plasma [11].

Plasma is a highly non-uniform system, and therefore, it is not in a state of thermodynamic equilibrium. Despite this, the principles of physics and the concept of local thermodynamic equilibrium (LTE) can still be applied to plasmas. This indicates that collisions occur more frequently than radiative transitions in plasmas. In the case of a system in LTE, McWhirter's criterion must hold true:

$$n_{\mathrm{e}} \geq 1.6 \cdot 10^{12} T^{\frac{1}{2}} (\Delta E)^3 \,, \tag{1}$$

where n_{e} (cm^{-3}) is the electron number density, T (°K) is the temperature of plasma and ΔE (10^{-7} J) is the highest energy transition for an isolated system [12].

If McWhirter's criterion (equation 1) is not satisfied, local thermodynamic equilibrium (LTE) cannot be established in the plasma. On the other hand, if the plasma is in LTE, it can be described using the Saha-Eggert relations, as well as the Boltzmann and Maxwell distributions [10].

The plasma temperature typically ranges in the order of several thousand Kelvin, and it can be determined, for instance, by analyzing the slope of the Boltzmann diagram. The electron density, on the other hand, can be measured using Stark broadening, whereby a higher spectral range of broadening corresponds to a higher electron density. It should be noted that the measurement of electron density is performed over a very short duration of time, while the temperature of the plasma remains constant [10].

Spectral line broadening can be caused by various factors, including collisions between particles, movement of electrons, and detector resolution. The impact of collisions on spectral line broadening depends on whether the collision is elastic or inelastic, with elastic collisions conserving energy but altering the phase of the radiation field, and inelastic collisions not conserving energy. The broadening of spectral lines due to propagation can be either uniform (Lorentzian curve) or non-uniform (Gaussian curve), and these may be combined to produce a Voigt curve that represents the actual spectral line. Therefore, when analyzing spectroscopic data, all factors that can contribute to the broadening of spectral lines must be considered, including collisions, electron movement, and detector resolution. Stark broadening is one type of spectral line broadening that can result in a Lorentzian curve, and it occurs due to electric fields from fast electrons and slow ions affecting atoms in a plasma plume. This broadens the energy levels and emitted wavelengths. On the other hand, Gaussian broadening occurs due to the Doppler effect caused by the thermal motion of atoms in the plasma, which causes a shift in the emitted light [13].

Spectrum is also time dependent. The spectrum of a plasma source changes over time and understanding its temporal behavior is important for analyzing spectroscopic data. Initially, the emission is dominated by a broad continuum radiation called Bremsstrahlung, which results from the thermal motion of electrons in the plasma. As the plasma cools down, the continuum radiation decreases and discrete emission lines become more prominent. The specific timing of the emission features depends on the type of species present in the plasma, with electron emission being stronger at an earlier stage and ion/molecule emission being stronger at later stages. Knowledge of the time-dependent behavior of a spectrum can provide insight into the physical processes occurring in the plasma source [14]. This can also be demonstrated in Figure 2.

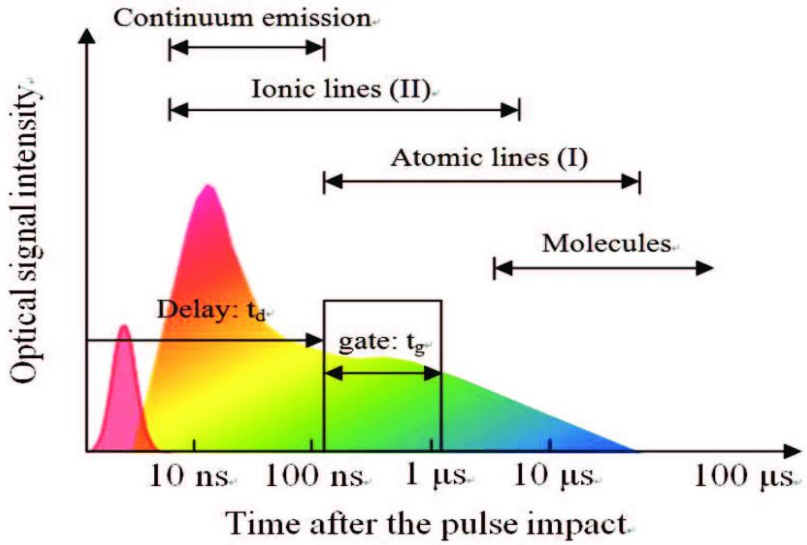

Figure 2: The standard temporal progression of plasma emission and the timing synchronization of the detector for both atoms and ions [15].

It should be kept in mind that various parameters such as the type of material in the sample or laser pulse properties can affect the formation of the plasma and the amount of material removed. Laser ablation is the process of removing specific portions of the sample surface and creating a plasma. Thermal, photochemical, and photophysical models are different types of ablation. The former is a type of ablation in which material is removed due to high temperatures. Thermal energy is converted from laser energy. Sometimes the bonds between molecules or atoms are broken, causing the material to ablate. This is photochemical ablation. The combination of these two models is called photophysical ablation. In LIBS, laser beam is focused on the surface of the sample and ionization of particles occurs after breaking the bonds between particles [16].

Each element possesses unique emission lines that can be identified and analyzed using the resource available at [17]. Additionally, it is important to note that each element exhibits multiple specific wavelengths. Although the LIBS spectrum may contain noise, it remains a valuable method for the detection of both atoms and molecules. For the purposes of this work, the focus is primarily on the identification of emitted heavy metal atoms, particularly lead [18]. The value for the chosen emission line of this element, specifically selected for this thesis, was obtained from the NIST website and is presented in Table 1. This particular wavelength was chosen for analysis in this thesis because it exhibits strong signal intensity and avoids interference from other high emission lines. For instance, even though there may be stronger emission lines available, the presence of calcium, which has significantly stronger emission lines, would potentially overshadow them.

Table 1: The selected emission line of lead (Pb) for analysis [17].

Pb I	Observed wavelength air (nm)	A_{ki} (s^{-1})	E_i (cm^{-1})	E_k (cm^{-1})
	405.78067	9.0^7	10 650.3271	35 287.2244

A_{ki} represents the Einstein coefficient for spontaneous emission , while E_i and E_k denote the energy levels of the lower and upper states of a transition, respectively.

LIBS experiments can be performed in various types of ambient gases, their pressure or even vacuum. Both the temperature and electron density of the plasma are affected by the **surrounding atmosphere**, not only by atmospheric pressure, but also by various elements in the type of ambient gas. The increase in atmospheric pressure around the plasma is directly proportional to the increase in temperature and density of electrons in the plasma and the signal intensity in the obtained spectrum. Elements from the ambient gas could cause molecular bonds to form between them and elements in the plasma plume [10].

It often happens that LIBS analysis gives a false result, that is, no signal is obtained even though the element is present in the sample. A situation where LIBS analysis may yield inaccurate results is when there is difficulty in distinguishing between the emission lines of two or more elements due to their similarity. In addition, if the surface of the sample is contaminated, this can interfere with the laser's ability to reach the sample and lead to inaccurate measurements, which can potentially impact the accuracy of the analysis [11].

The limit of detection (LOD) is also a critical figure of merit that represents the lowest concentration of an element that can be detected. The formula used to calculate the LOD is:

$$\mathrm{LOD} = \frac{3\sigma}{b}, \tag{2}$$

where b is the slope of the calibration curve, σ is the standard deviation of the background or reference sample and this quantity is multiplied by the number three because 3σ contains 99 % of the results of the reference sample [5]. Signal stronger then 3σ can be assigned to the certain element.

Another important formula used to calculate LOD is:

$$\mathrm{LOD} = \frac{3cSD}{\overline{X_{\mathrm{Pb}}}}, \tag{3}$$

where c denotes the element's concentration, and SD stands for the background's standard deviation, which is multiplied by three to obtain 99 % of the reference sample's results. $\overline{X_{\mathrm{Pb}}}$ refers to average element response due to signal and background [5].

Laser pulse length is another parameter that affects the physical and chemical properties of plasma. The two mainly used types of lasers in LIBS are femtosecond (fs) and nanosecond (ns) lasers. It is also possible to utilize picosecond lasers (ps) for various purposes, but they are less commonly used. Nanosecond lasers are more widely used due to their more affordable prices. These types of lasers can cause very different properties of plasma. In the context of material ablation, nanosecond laser pulses may produce a plasma plume that can lead to imprecise ablation craters and thermal damage. On the other hand, femtosecond lasers typically create a Coulomb explosion instead of a plasma plume, resulting in the formation of craters with greater precision and minimal thermal damage. Femtosecond lasers also create cooler temperatures for the plasma plume [10].

Although using these two lasers results in different signal intensities, similar results can be obtained if we optimize the irradiance, i.e. if we use lower irradiance for the nanosecond laser and higher irradiance for the femtosecond laser. The ablation patterns of these two lasers are shown in Figure 3.

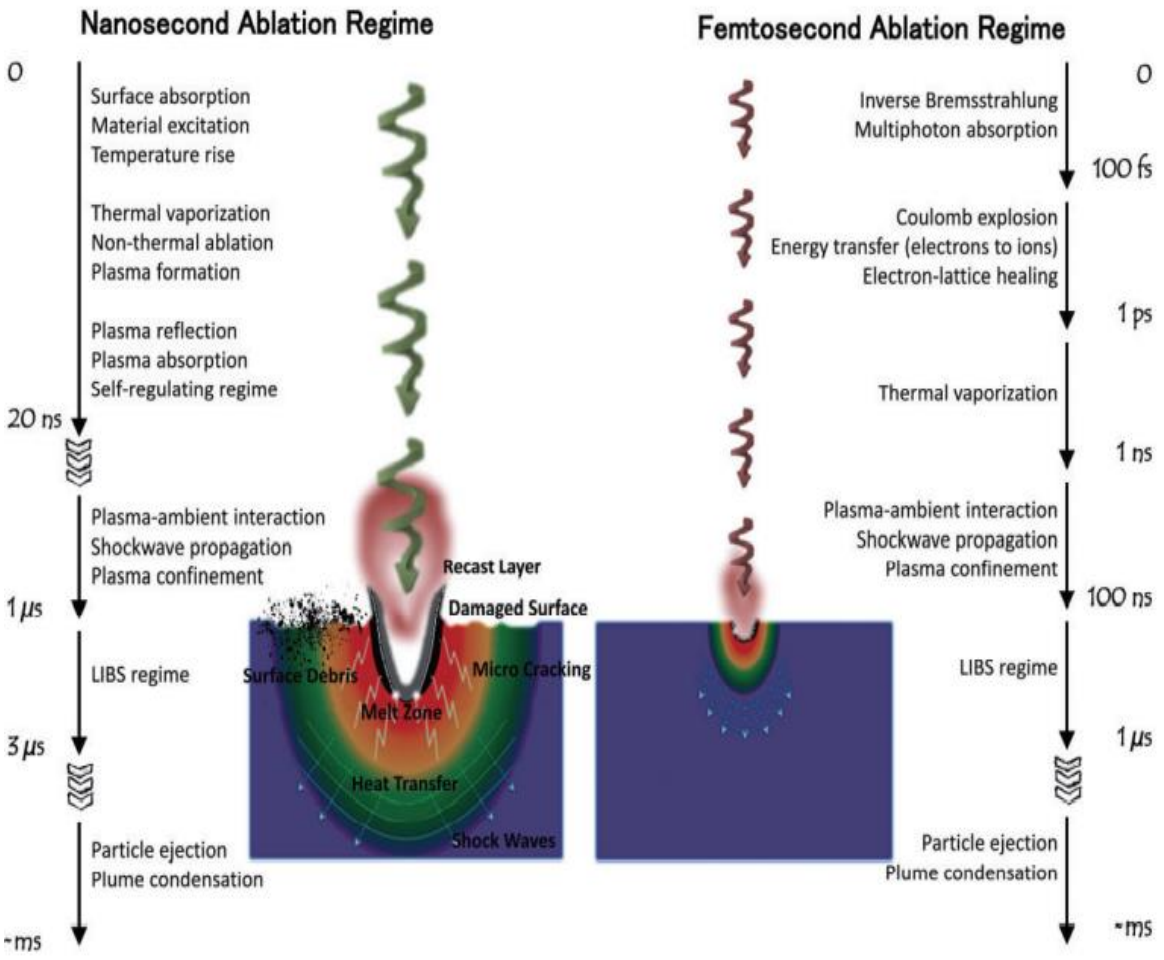

Figure 3: Nanosecond and Femtosecond Ablation Regime [16].

Most LIBS studies are performed using a pulsed nanosecond Nd:YAG with **pulse wavelength** of 1064 nm, which corresponds to the infrared spectrum. Lasers with wavelengths of 532 nm and 266 nm are also used for this type of laser. The laser wavelengths of 266 nm and 532 nm are derived by means of frequency doubling, a procedure that entails the use of a nonlinear crystal to convert the fundamental wavelength of 1064 nm into shorter wavelengths. As a result of this process, a second harmonic at 532 nm and a fourth harmonic at 266 nm are produced. In general, the smallest craters are those produced with the lowest wavelength of the three. In this work, the performance of these three wavelengths was compared during the analysis of Pb [19].

In addition to atmospheric conditions, laser pulse wavelength, and laser pulse duration, the signal intensity in LIBS is influenced by other parameters such as **gate delay, interpulse delay, laser energy, and laser focus**. In this thesis, these parameters were varied along with the laser wavelength to optimize the results.

Gate delay is the delay time between the laser pulse and the time the detector records the signal [20]. Critical aspect is also the laser pulse energy, which directly influences the irradiance generated. The time delay used between two pulses in double-pulse LIBS is called interpulse delay (ID).

There are two distinct types of defocus utilized in LIBS, specifically positive and negative defocus. Negative defocus entails a deviation of the laser focus in the negative direction relative to the tight focus point, meaning that the distance between the laser lens

and the sample surface is smaller than the focal length of the lens. Conversely, positive defocus refers to a shift of the laser focus in the positive direction. Typically, negative defocus leads to a reduction in the laser beam size, resulting in a higher laser intensity and a smaller spot size. Optimizing LIBS performance is contingent upon the proper application of defocus strategies, which are dependent on the particular experimental conditions and material characteristics under investigation [21].

2.2.2 Instrumentation for LIBS

LIBS consists of four main components: laser, optical system, spectrometer, and the control electronics (such as softwares used to process data) [10]. An example of LIBS instrumentation can be seen in Figure 4.

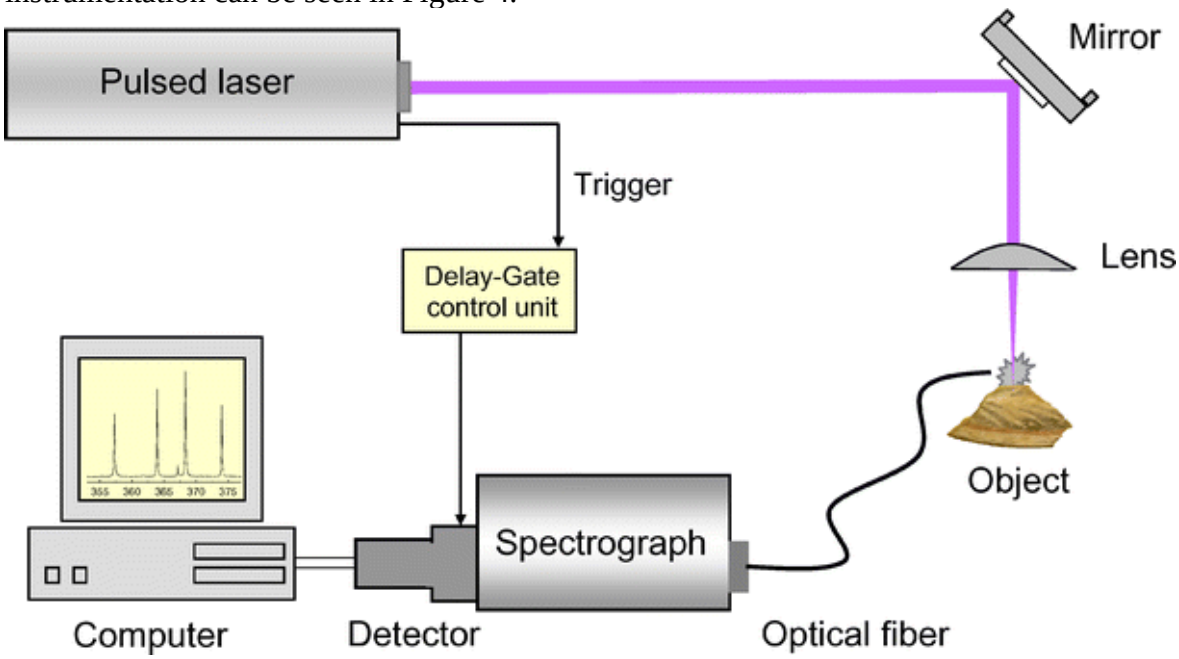

Figure 4: LIBS instrumentation [22].

Lasers can be divided based on several criteria such as laser pumping and type of active material. They are divided into solid-state, fiber, gas, excimer and ion lasers. The most commonly used lasers in LIBS are solid-state lasers, with gas and fiber lasers as secondary options, although other laser types such as dye, excimer, and CO_2 have also been utilized. LIBS lasers mainly have yttrium-aluminum garnet as active material and are doped with positive Nd ions. The basic properties of the laser are coherence, monochromaticity and collimation. The lowest-order mode of the laser beam is a Gaussian beam. It is defined by the divergence and curvature of the wave fronts [23].

The majority of lasers utilized in LIBS configurations are Q-switched Nd:YAG lasers with nanosecond pulse durations. LIBS generally uses electro-optical type of resonator switching. The technique of Q-switching (utilizing an optical switch, either electro-optic or acousto-optic) in Nd:YAG lasers is an efficient technique for generating high-energy light **pulses** in lasers [23]. This technique works by controlling the laser cavity's quality factor (Q-factor), which determines the efficiency of energy storage and release in the form of light. The Q-switch changes the duration of energy storage and release, leading to longer storage times and higher energy states or a rapid burst of light with a low-quality factor [24–25].

A suitable lens, or in more advanced systems a set of lenses, is used to focus the laser beam onto the sample. It is also used to collect the light emitted by the plasma. Recently,

fiber optic technology has advanced significantly, leading to the creation of fiber optic LIBS. A laser beam can be sent from the laser to the sample surface via an optical fiber, and light from the plasma can also be transmitted to the detector via an optical fiber. Usually only one fiber is used instead of two [18].

The emitted radiation is resolved into specific wavelengths using **a spectrometer** with the help of dispersive elements (optical prisms or gratings). Paschen-Runge, Czerny-Tuner and Echelle spectrometers are spectrometers that have been used in LIBS setups. Echelle spectrometers are superior to the other two because of their wider spectral range. Paschen-Runge spectrometers are rarely used nowadays [10].

The principle of Czerny-Turner's work is that the incident light is made parallel by the collimating mirror before being split into its various wavelengths through the diffraction grating. Czerny-Turner is the spectroscope used in our laboratory. Its schematic representation is shown in Figure 5. M_1 and M_2 are concave mirrors [18].

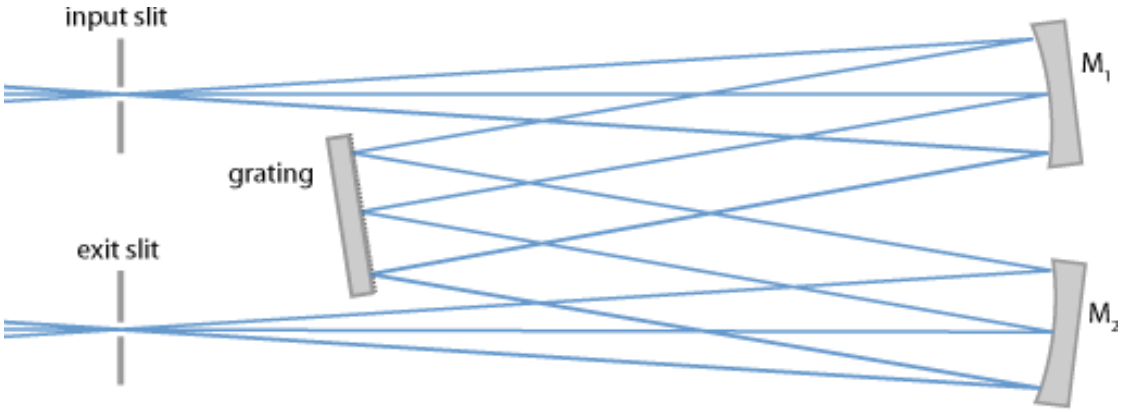

Figure 5: Setup of a Czerny–Turner spectroscope [26].

A wide range of wavelengths is crucial for analyzing multiple elements in a sample. In Echelle spectrometers, Charge Coupled Devices (CCDs) are the preferred detectors as they can record radiation intensity as a function of wavelength. Photomultiplier tubes (PMTs) and photodiode arrays (PDAs) are also used in LIBS analysis, but CCDs provide the best signal-to-noise ratio and sensitivity. Intensified CCDs (ICCDs) are a specialized version of CCDs. They have multichannel plate in front of the detector, that is capable to intensify (increase the amount of electrons) the signal based on applied voltage. Alternatively, metal-oxide-semiconductor (CMOS) sensors can also be utilized for detecting signals. The selection of the detector relies on the specific requirements of the analysis as well as the equipment that is available [18].

2.2.3 LIBS signal enhancement

There are several ways to improve the limits of detection of LIBS. Physical methods are: multiple pulse methods, such as double-pulse LIBS (DP-LIBS), spatial constraint and magnetic constraint method and atmosphere control method. Chemical enhancement methods is, for example, chemical replacement method. Nanomaterials can be used as an enhancement technique in both physical and chemical ways to improve the analytical performance of LIBS [27].

Multi-pulse LIBS usually offers enhanced signal to noise ratio (SNR) and signal to background ratio (SBR) when compared to single-pulse LIBS [11]. SNR measures the magnitude of the signal against the noise level, while SBR measures the signal level

against the background level. Greater SNR and SBR lead to improved precision and sensitivity, a more powerful signal and less noise. Some possible DP-LIBS configurations are shown in Figure 6.

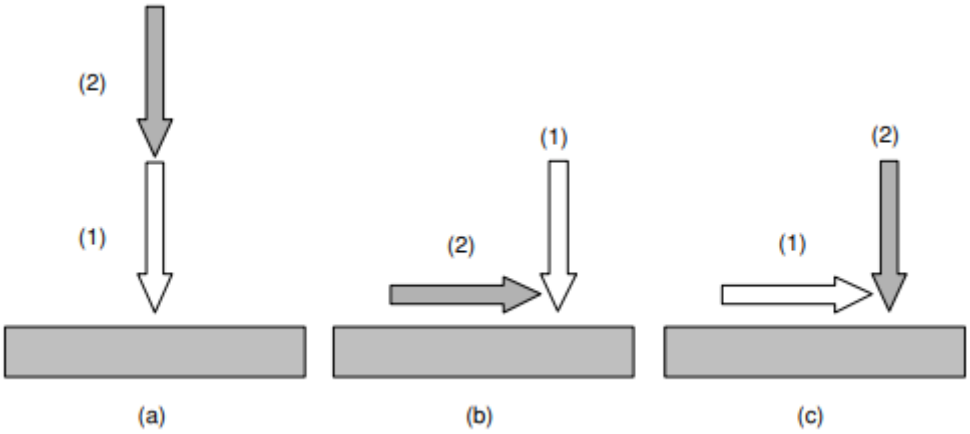

Figure 6: Types of configurations of DP-LIBS. (a) collinear; (b) orthogonal reheating; (c)orthogonal pre-ablation configuration [11].

Nowadays, two lasers are usually used for DP-LIBS, although only one laser can be used. While using a single laser is generally more cost-effective in terms of configuration cost, employing two lasers typically provides a higher level of precision in DP-LIBS.

With a collinear configuration, we must ensure that both laser beams pass the same path but with a time difference, and that they are focused on the same spot in terms of position on the sample. The two orthogonal modes used are the reheating and pre-ablation modes. In the reheating mode, sample ablation first occurs with the first pulse that is focused on the sample, and then the second pulse that is parallel to the sample reheats the plasma plume. In the pre-ablation mode, it is the other way around, the initial laser pulse removes the air or gas above the sample surface by ablating it, which creates a small region of vacuum-like conditions. Subsequently, a second laser pulse is used to ablate the sample itself. There are some other, less-used, configurations of laser beams, in one of them two laser beams fall on the sample at an angle of 45 degrees to the sample and with a right angle between beams [18].

DP-LIBS often uses lasers of different wavelengths. If the two laser pulses used in DP-LIBS have different wavelengths, it allows the first laser pulse to remove a small amount of material from the sample surface, and it also creates a plasma that has a high concentration of electrons. The second laser pulse, which typically has a shorter wavelength, can then be used to stimulate this electron-rich plasma, producing emission spectra that are more intense and well-resolved [18].

DP-LIBS is a widely used technique, but it is also possible to use more than two pulses (triple-pulse LIBS). The setup of this method was reported in a publication by Prochazka et al. and is shown in Figure 7 [28].

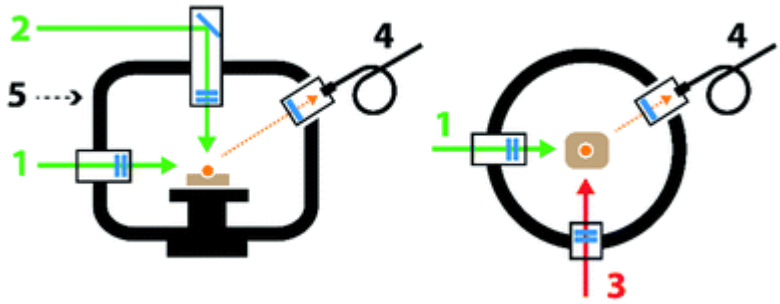

Figure 7: The diagram depicts two schematic images showing the interaction chambre from a front view (on the left) and a top view (on the right). The chamber consists of laser pulses and collection optics. All laser pulses are oriented perpendicular to each other. The ablation pulse (2) is emitted from the top of the chamber (5), directed perpendicular to the surface of the sample. The pre-ablation pulse (1) originates from the left side of the chamber (5) and aligns with the sample surface. The re-heating pulse (3) is directed from the front of the chamber (5) and is collinear with the sample surface. The collection optics (4) are positioned on the right side of the chamber [28].

2.2.4 Data processing in LIBS

In the previous sections, qualitative and quantitative analysis using LIBS was discussed briefly. Qualitative analysis involves identifying the presence or absence of specific elements or compounds in the sample based on their characteristic spectral lines, which are compared with known spectral databases. Single-pulse LIBS is generally sufficient for qualitative analysis. Quantitative analysis, on the other hand, is concerned with determining the concentration of a particular element or compound in the sample. The concentration is established by correlating the intensity of the spectral line of interest with the known concentration of that element in standard samples. Calibration curves are generated by analyzing standard samples with known concentrations of the element of interest. Quantitative analysis can also be performed using chemometric methods, which involve statistical analysis of the spectra to identify the elemental composition of the sample [29].

Chemometric methods include principal component analysis (PCA), partial least squares regression (PLS), and artificial neural networks (ANN), and can analyze complex spectra containing multiple spectral lines. In addition to qualitative and quantitative analysis, data processing in LIBS involves pre-processing and scaling of the spectra, automatic selection of spectral lines, and image fusion [30].

Two modes of 2D analysis are available when using LIBS: step-by-step scanning and continuous scanning. Step-by-step scanning entails scanning the sample point-by-point, which can be time-consuming. In contrast, continuous scanning only allows for single-shot analysis and does not provide the ability to focus on a specific point due to the nature of the scanning mechanism. As a result, the laser beam covers a wider area of the sample, making it difficult to focus on a specific point [31]. Ablation spots can overlap each other, but this is not necessary for the analysis. If the distance between the two spots and the size of the spots are chosen so that they overlap each other, a better resolution image is obtained.

LIBS enables hyperspectral imaging, where each point on the sample is represented by a spectrum of spectral (λ) and spatial (x, y) information. The resulting 3D dataset can be

used for various types of analysis. For example, chemometric methods can be applied to extract useful information from the dataset. The first step in data processing is often the translation of the 3D dataset into 2D, which is useful for creating elemental maps. Pre-processing techniques such as normalization and background subtraction can be applied to the individual spectra before calculating the intensity of a spectral line. Automatic peak selection methods, such as the image features assisted line selection (IFALS), can be used to select spectral lines, especially when dealing with full LIBS spectra that contain hundreds of lines. After pre-processing and scaling, the data can be analyzed and visualized using a multisensor imaging tool. While reducing the 3D hyperspectral dataset to 2D is often done for visualization purposes or further analysis, it is not always necessary and the data can also be approached individually from the start. LIBS-based hyperspectral imaging has the potential for various applications in the biological imaging of soft and hard tissues [31].

2.3 Biomedical applications of LIBS

As mentioned earlier, this thesis is about LIBS analysis of hard tissues (i.e. teeth and bones). The main mineral that makes up hard tissue is hydroxyapatite ($Ca_{10}(PO_4)_6(OH)_2$) [32]. In addition, LIBS is also useful in soft tissue analysis. An example of why elemental analysis of tissues is important is that some elements, such as Pb and Cd, are toxic to living organisms, while others, such as Mg and Fe, are essential for normal organism function (but can also become hazardous at certain concentrations). Therefore, LIBS analysis can determine whether a tissue contains an optimal concentration of an element. Additionally, many studies have looked at detecting cancer using LIBS technology by monitoring differences between healthy and diseased tissue. For example, a lower concentration of calcium in the bone could lead to bone decalcification and furthermore to origin of osteoporosis, while a higher concentration of calcium in soft tissues may suggest the presence of cancer. Chapter 2.3.2 of the thesis offers a more comprehensive examination of the pertinent problematic, accompanied by the relevant citations [36, 37, 38].

Optimizing the pulsed laser wavelength is critical for mapping biological tissues. Water is the primary absorber in soft tissues, leading to the highest absorption rates in the UV and far-IR regions. In contrast, hard tissues, such as teeth, absorb radiation most efficiently in the visible and near-infrared regions. Figure 8 illustrates the absorption curves of tooth tissue components at various laser wavelengths, with the Er:YAG laser generating the most significant absorption at around 2900 nm, followed by CO_2 laser radiation at 10,600 nm. However, the absorption dependence varies among different tooth tissues, emphasizing the need for laser wavelength selection based on the tissue's optical properties for accurate analysis [32].

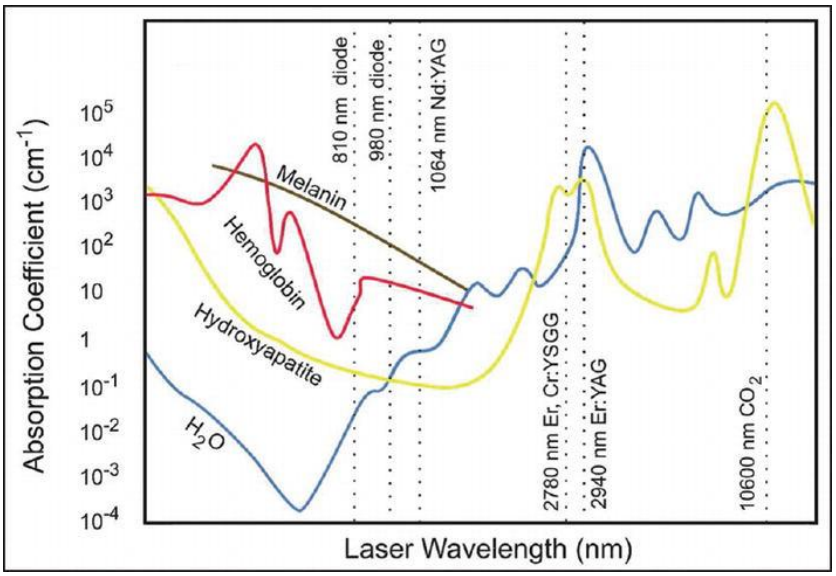

Figure 8: An examination of the absorption properties of laser beams in relation to different wavelengths conducted for the primary constituents found within the structure of a tooth [32].

2.3.1 Teeth

A tissue is a group of cells that are interconnected and have similar properties. There are four types of tissue: muscular, nervous, epithelial, and connective. Teeth are composed of connective, hard (have high degree of hardness) tissues: **enamel, dentin, and cementum**. The main function of teeth is to cut food. The lower jaw and upper jaw support the two rows of teeth and the nose. Humans have 32 teeth (8 incisors, 4 cuspids, 8 bicuspids and 12 molars). A tooth consists of three parts: the crown, neck, and root. The structure of the tooth is shown in Figure 9. The crown is the functional and visible part of the tooth, mainly composed of dentin, blood vessels and nerves (pulp), and covered with enamel. The neck connects the crown and root of the tooth. The root, like the crown, is made of dentin covered with cementum, and this is the invisible part of the tooth. Root canals are also part of it and are made of blood vessels and nerves [33].

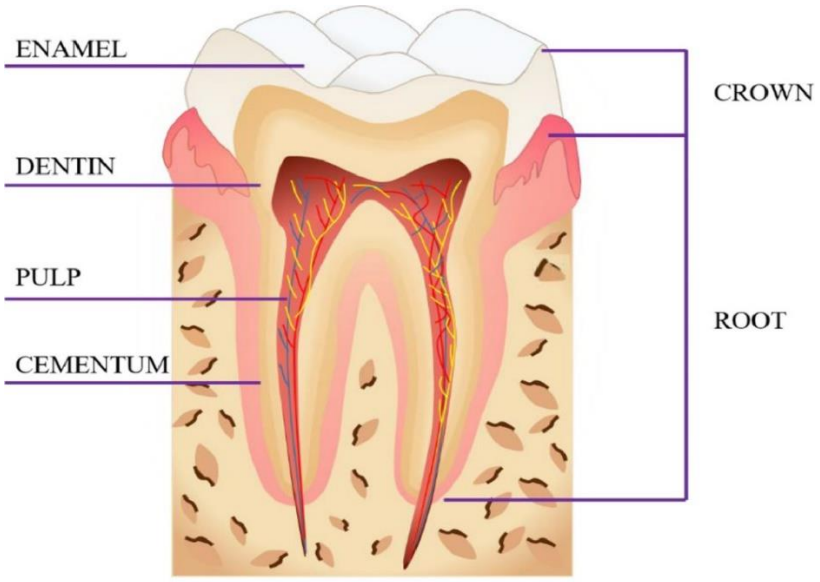

Figure 9: Tooth anatomy [34].

The basic function of tooth enamel is to protect the vulnerable parts of the tooth. This part is made up of about 95 % minerals and about 3 % water. Dentin is a hard tissue found under tooth enamel and is made up of about 70 % minerals. Cementum is a hard tissue, similar in composition to bone, that connects the pulp to the tooth. It consists of approximately 45 % minerals. Another tissue that makes up teeth is dental pulp. However, in contrast to the first three tissues listed, dental pulp is not a hard tissue but a soft tissue. It consists of blood vessels, lymphatic vessels, and nerves [33].

Animal tissues, especially those of mice, are frequently used as a first step in research experiments due to their fast reproductive rate and anatomical resemblance to humans, particularly in their bone and teeth structure. However, relying solely on animal models is not always ethical, although this approach has helped to expand the technique's usefulness in analyzing human tissues. Human teeth differ from those of mice in several ways, such as humans having 32 permanent teeth while mice only have 18. Additionally, mice do not have primary teeth and possess only permanent teeth throughout their lifespan [35].

While LIBS is commonly used for the analysis of teeth and bones, detecting heavy metals in bones can be more difficult than in teeth due to the lower amount of hard tissue present. Therefore, a different approach may be necessary to achieve accurate heavy metal detection in bone tissue using LIBS.

2.3.2 Heavy metals and their impact on human health

Heavy metals is the name used to denote elements harmful to the human body. Although heavy metals can be useful in some quantities, they are mostly very toxic after a certain concentration. In general, the opinion is valid that in order for an element to be considered a heavy metal, it must have a density of over $5\ \mathrm{g/cm^3}$. Some of these metals are arsenic, lead, cadmium, and copper [36].

Exposure to heavy metals, including lead, cadmium, mercury, and arsenic, can have significant harmful effects on living organisms and pose a major public health concern. These metals can accumulate in the body through various sources, such as industrial activities, contaminated food and water, and cigarette smoking. Long-term exposure to these elements can result in severe health problems, including damage to the nervous, cardiovascular, and renal systems, harm to bone tissue, and even cancer. Cadmium, in particular, is known to cause painful joint movement due to its effects on bone tissues. Lead is concerning due to its potential for harm to cognitive development, especially in children. Thus, detecting and measuring lead levels in biological samples is crucial for assessing potential health risks associated with lead exposure. This thesis aims to detect and quantify lead using LIBS technology in biological samples, providing an effective means of assessing potential health risks associated with lead exposure [37].

Lead (Pb) is a heavy metal with an atomic mass of 207.2. Its atomic number is 82. There are organic and inorganic forms of lead, organic lead is more toxic. Its concentration in the environment has decreased over the past years due to the use of unleaded gasoline, but it is still very much present in quantities that exceed the limit of being harmless to humans [38].

The biggest intake of lead is through inhalation. This element binds to enzymes in the body and thus interferes with the normal functioning of cells. Lead can often be found in water, especially in households with weak water installations. Some of the first symptoms of lead poisoning are insomnia, decreased appetite, and headache. If lead poisoning occurs, milk, whose proteins bind lead, has proven to be an effective remedy [37].

3 State of the Art: An overview of the current status of knowledge

The analysis of hard tissues, the detection of toxic elements in the tissue, the improvement of the signal using the multi-pulse LIBS method, as well as the comparison of different laser wavelengths are areas that many scientists have already been interested in. Some of the research that has been done in the past is listed in the following chapters. To the best of the author's knowledge, no previous study has examined the combined influence of different laser wavelengths on the detection of heavy metals in hard tissues. The aim of this work is to contribute to the optimization of parameters for the three laser wavelengths, which should contribute to easy and improved analysis of hard tissues in the future.

3.1 Analysis of biological tissues by LIBS

3.1.1 Analysis of soft tissues by LIBS

In 2023 Winnand et al. were able to discriminate bone-invasive oral cancer from healthy tissue using 1064 nm nanosecond Q-switched Nd:YAG laser [39]. They observed electrolyte balance of calcium (Ca), potassium (K) and sodium (Na) in cells of human mandibular specimens, which were obtained through surgery with the written consent of the patients and ethical approval. Although the mandible is considered hard tissue, the analysis performed in this study focused on cells extracted from the mandibular specimens, indicating that it pertains to soft tissue. This paper also mentions a comparison with experiments in which Ca, Na and K were detected by LIBS analysis on samples of the mandible in pigs. They showed similar results to this research conducted on human mandibles. A change in the balance of the mentioned electrolytes can be caused by conditions such as vomiting or long-term diseases such as a tumor.

In this experiment, 15 patient samples were analyzed using LIBS. The samples were prepared by drying for 12 hours, cutting into 4-mm thick sections with tumorous areas embedded in paraffin, and cleaning with NaCl before analysis. The emitted radiation was collected by a spectrometer covering 200–870 nm, and LIBS analysis required 30 shots per spot.

The study found a low Ca signal in tumorous tissue, while the Na and K signal intensities were increased with an overall sensitivity of 96 %. These findings are shown in Figure 10.

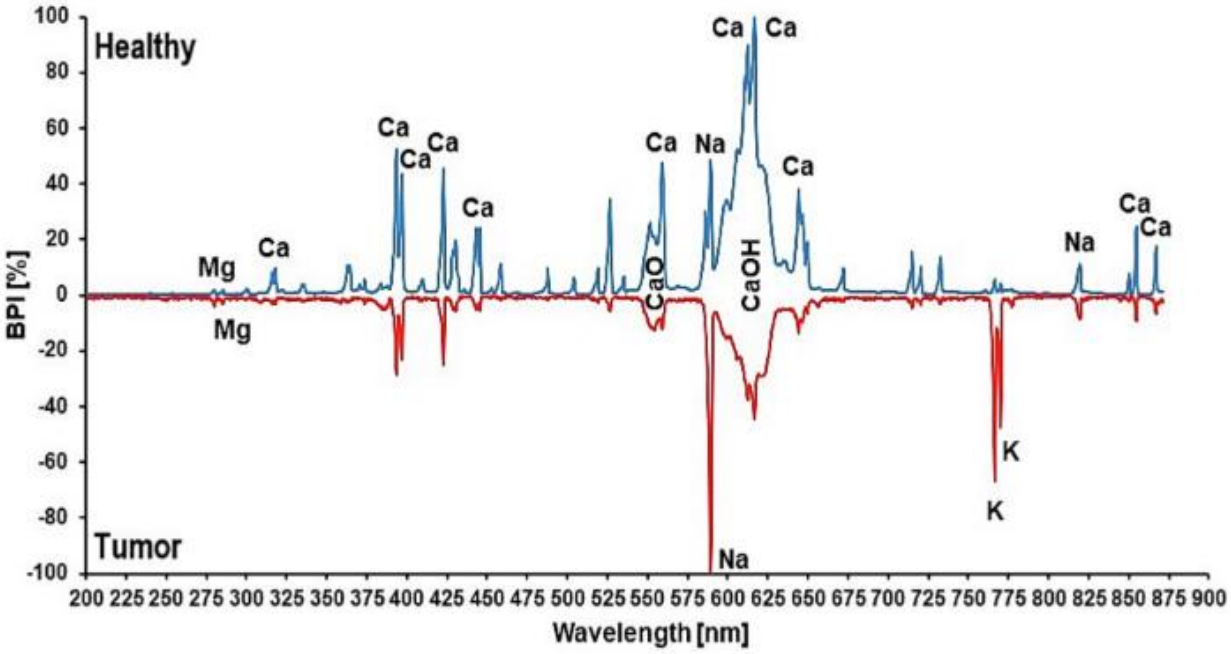

Figure 10: Distinctive spectral profiles of normal bone (blue) and bone-invasive oral cancer (red) [39].

The result of this research proved that it is possible to do real-time LIBS analysis of tumorous tissue, which almost does not require sample preparation and it opens up many new possibilities in the field of biomarker studies.

3.1.2 Analysis of hard tissues by LIBS

Alicia Marín-Roldán et al. [40] conducted a study in which they employed calibration-free LIBS (CF-LIBS) to analyze the elemental composition of a complex matrix of a wild boar rib bone that contains both major and minor elements. They utilized the NIST LIBS application to simulate plasma cooling and calculated the intensities of emission lines under different conditions to optimize the Saha-Boltzmann plot. They identified suitable lines of elements such as Ca, Mg, P, Sr, O, and H, and measured the plasma temperature at different delays. The study utilized a Q-Switched Nd:YAG laser with a wavelength of 266 nm to analyze the flat part of a wild boar's ribs. Emission lines were captured by both VUV and Echelle spectrometers. By calculating the atomic and mass percentages of Ca and P, they determined the Ca/P ratio. The Ca/P ratio is an essential metric for assessing compatibility with human bones, and trace elements like magnesium and strontium can offer insight into various factors such as diet. This approach provides a reliable, non-invasive, and pre-treatment-free means of analyzing bone composition and has potential implications for understanding diet and biocompatibility with human bones.

The Ca/P ratio calculated for delay times of 500 ns and 1000 ns, as well as the calculated values for the atomic and mass percentages of the analyzed elements, are presented in Table 2.

Table 2: Elements selected along with their atomic and mass percentages in a bone sample, as well as the Ca/P ratio, at delay times of 500 ns and 1000 ns [40].

Element	500 ns		1000 ns	
	Atomic %	Mass %	Atomic %	Mass %
Ca	21 ± 1	37 ± 3	20 ± 7	35 ± 3
P	13 ± 4	18 ± 5	17 ± 3	23 ± 4
Mg	6 ± 3	7 ± 3	5 ± 2	5 ± 2
Sr	0.014 ± 0.003	0.05 ± 0.01	0.02 ± 0.02	0.07 ± 0.01
O	55 ± 3	38 ± 3	53 ± 8	36 ± 3
H	4.2 ± 0.3	0.18 ± 0.01	4 ± 2	0.18 ± 0.01
Ca/P ratio	1.6 ± 0.4	2.1 ± 0.4	1.2 ± 0.5	1.5 ± 0.3

Notably, the results indicate that the Ca/P ratio calculated at a delay time of 500 ns is more precise. The study also showed that in this case CF-LIBS is advantageous over LIBS for compositional analysis as it simplifies the process and eliminates the need for a calibration plot. It also reduces the error associated with spectral line variation, making it faster and more reliable for quantitative analysis.

3.2 Heavy metal detection

During the research for the thesis, the author noted a scarcity of literature pertaining to the analysis of heavy metals in hard tissues using LIBS. However, Samec et al.'s research [41] somewhat delved into this topic by analyzing the accumulation of metals such as aluminum in hard tissues.

The researchers utilized a Nd:YAG laser with a wavelength of 1064 nm for their study, ensuring that the laser energy did not exceed 20 mJ to prevent destruction of the sample and large ablation craters. This is particularly significant because the samples used in the study were teeth samples. The researchers employed depth profiling LIBS analysis on these samples, primarily limited to the surface layer due to the geometric restrictions of plasma on deeper depths. Depth profiling involves ablation of the sample layer by layer, whereas cross-sectional analysis was also carried out by cutting thin layers of samples to generate 2D distributional maps of the analyzed elements in teeth samples. The elements studied included Ag, Al, Ca, Cr, Hg, K, Mg, Mn, Na, Ni, P, Sn, Ti, and Zn.

Furthermore, the researchers compared and analyzed teeth from various age categories, ranging from infants to adults, for the element Al. However, the primary objective of the study, conducted in 1999, was to demonstrate the possibility of detecting elements in hard tissues, rather than to establish a trend between different age categories. The study revealed the presence of Al in approximately 30 % of samples, proving that LIBS is an effective tool for detecting metal accumulation in hard tissues.

Gallstones form in the gallbladder and cause blockage of the digestive system. Its diameter is 2–5 mm. The largest compound of gallstones is cholesterol. Its analysis is essential for the diagnosis of the patient. Naser et al. [42] used 1064 nm nanosecond Q-switched Nd:YAG laser to do quantitative analysis of heavy metals in gallstone, such as Cr, Pb, Zn, As, Cu and Cd. Laser energy was set to 300 mJ. The emission spectrum was collected with an optical spectrometer with a built-in CCD camera that had a range of 200–1100 nm. A total of 12 samples collected from patients of different genders, ages and from different

hospitals were used for the analysis. Six samples were used to create the calibration curve. Almost no sample preparation was needed. They were dried in furnance. The concentration of heavy metals in them was accurately determined by atomic absorption spectrometry (AAS) analysis. The calibration curve was used for the quantitative analysis of the remaining 6 gallstones on which AAS analysis was not performed.

Heavy metals were detected at wavelengths between 250 and 650 nm. The two spectral lines that are interesting for my thesis are for Pb and Cd. For their analysis, the authors used spectral lines at 357.27 nm and 441.56 nm, respectively. An example of the spectrum obtained from the analysis of gallstone marked with the abbreviation GS6, taken from a 65-year-old male patient, can be seen in Figure 11.

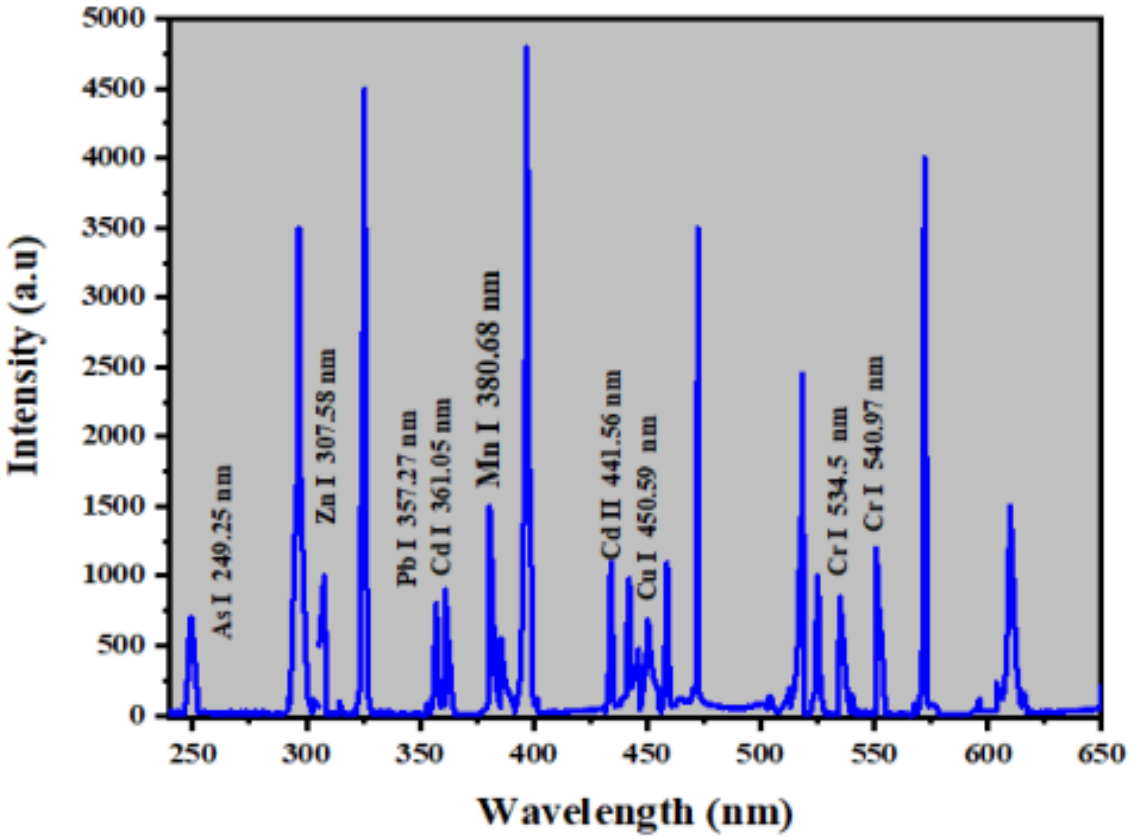

Figure 11: The spectrum obtained by measuring the sample GS6 [42].

Quantitative analysis was done by first measuring the concentration of heavy metals in 6 samples using AAS analysis, and then measuring the signal intensity of these same elements using the LIBS method. A calibration curve was created, i.e. the dependence of intensity (y axis) on concentration (x axis). It is a linear dependence and can be seen in Figure 12.

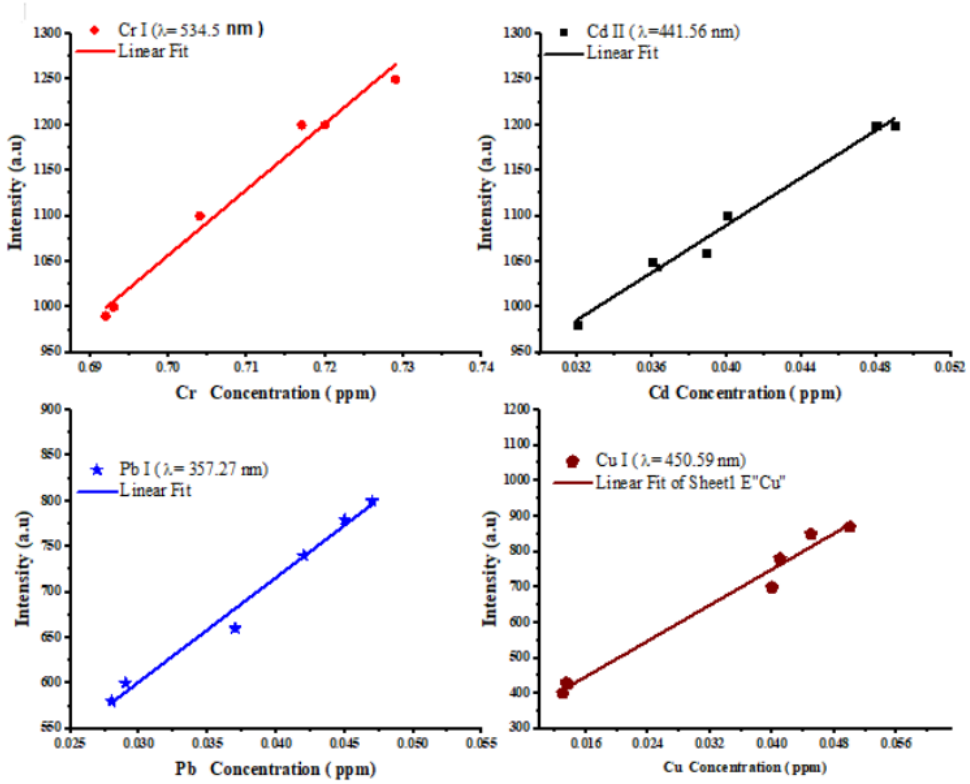

Figure 12: Calibration curves of individual detected elements [42].

Based on the calibration curve, the concentration of heavy metals was calculated for the remaining 6 samples that were analyzed only by the LIBS method. It is important to mention that at the end of the research, 6 samples that were initially measured only by the LIBS method were measured by the AAS method as well and the concentration almost completely corresponded to the concentration measured by the qualitative LIBS analysis. This means that LIBS analysis can be used with great accuracy for the qualitative analysis of heavy metal in gallstones. It was also concluded that the heavy metals Pb and As had a much higher signal intensity, i.e. concentration in samples taken from patients who were smokers.

In 2022 Honglian et al. [43] investigated temperature control and the influence of KCl additives on the detection of heavy metals in sediment samples by LIBS analysis. The samples were collected next to Baiyang Lake in China. Soil pollution with heavy metals is, as mentioned earlier, a very important factor that affects the development of plants. If a person uses plants from contaminated soil in his diet, this can lead to the appearance of various diseases.

A 1064 nm nanosecond Q-switched Nd:YAG laser was used for the analysis. Aperture was set to 6 mm, and a spectrometer with a built-in CCD camera that had a range of 199–517 nm was used. Frequency was set to 5 Hz. The spectral line used for Cd detection was at a wavelength of 228.8 nm. The wavelength 405.78 nm was used for Pb. 7 mm thick, naturally dried samples were treated with different amounts (0 %-100 %) of KCl additives.

The measurements were first carried out at room temperature, for different concentrations of KCl additives in the sediments. It was discovered that the best signal, as well as the signal to noise ratio (SNR), was at a content of 15 %. The signal weakened again by a larger percentage. After that, the analysis was done again for the samples that had this

concentration, but this time the temperature of the substrate was set to 180 °C. This further improved signal intensity and SNR. For example, when the Cd signal was measured without added additives at room temperature, the signal intensity of this heavy metal measured by LIBS was 6 484 arb. u., while with 15 % KCl additive it was 11 073 arb. u. The SNR value changed from 22.8 to 31.9. When the Cd signal was measured at 180 °C substrate temperature without additives, the signal intensity was 10 765 arb. u. and SNR value 28.9. When the Cd signal was measured at 180 °C with 15 % KCl additive, the signal intensity was 13 025 arb. u. and the SNR value was 40.5.

The results of this work marked the LIBS method as a very effective method for the analysis of toxic substances in soil. What improves SNR and signal intensity is the addition of additives and changing the temperature of the substrate. In the case of the experiments conducted in this research, the optimal combination of additives and temperature resulted in signal enhancement up to 2.01 times, and SNR up to 1.78 times.

3.3 Influence of different laser wavelengths on LIBS analysis of hard tissues

In 2014, M.A. Kasem et al. [44] conducted a study on the influence of laser wavelength on the analysis of archeological bone using LIBS methods. The researchers compared the performance of 1064 and 266 laser wavelengths. To obtain samples, bone fragments from four Egyptian dynasties were ground and pressed into homogenous bone pellets to ensure reproducibility. The researchers also obtained a standard bone ash sample from the National Institute of Standards and Technologies for use as a reference material. The experimental conditions for the two systems were kept similar, with laser energy, spot size, repetition rate, and irradiance controlled. Detailed descriptions of the instruments used are provided in [44].

The results of the study showed that the 266 nm excitation wavelength provided more consistent results for the measurement of Sr and Mg elemental intensity within the same dynasty. The relative standard deviation (RSD) values were generally lower for the 266 nm excitation wavelength, indicating lower variability between individual samples. This suggests that the 266 nm excitation wavelength may be a more reliable method for analyzing ancient bone samples. The comparison of the intensities and RSD values within the same dynasty is depicted in Figure 13.

Conducting a UV-LIBS analysis on elemental changes within a particular dynasty is crucial in obtaining a dependable understanding of the health status and dietary patterns during those ancient times. The study employed two different laser excitation wavelengths to measure the depth profile of bone samples and found that UV-LIBS provided plasma properties that closely resembled the bone ash standard reference sample utilized for calibration, indicating greater stability. Moreover, measuring strontium concentration relative to calcium through depth profiling can serve as an indicator of the diagenesis effect caused by the surrounding postmortem environment.

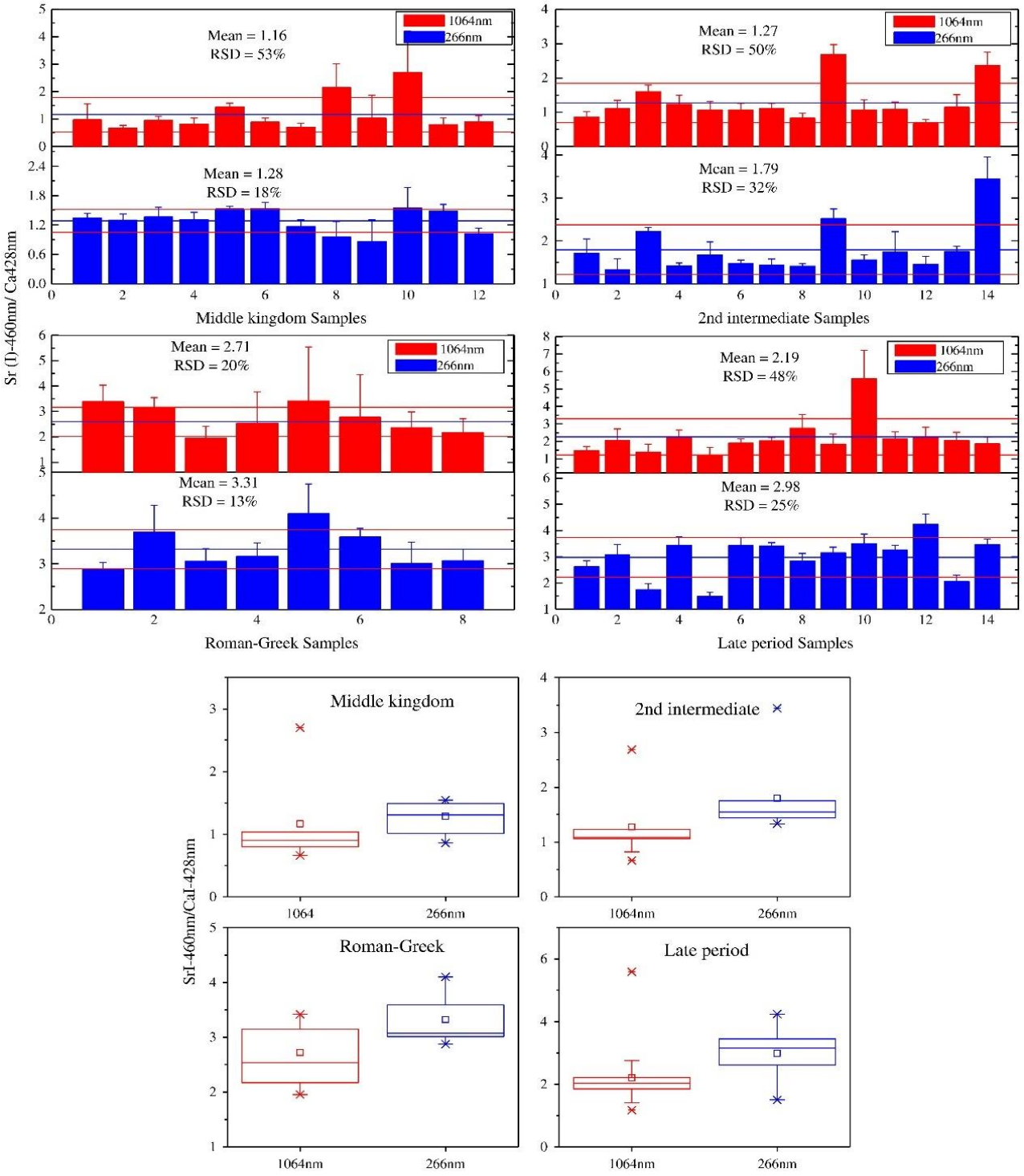

Figure 13: Elemental fluctuation of (Sr) within the same dynasty [44].

4 Experimental section

4.1 Used chemicals

- Argon, purity of 99.996 % (SIAD, Prague, Czech Republic)

4.2 Used equipment and software

4.2.1 Used equipment

- LIBS FireFly (Lightigo, Brno, Czech Republic)
- LIBS Discovery (CEITEC, Brno, Czech Republic)
    - Nd:YAG laser, 532 nm, CFR Ultra, laser pulse 10 ns (Quantel, Lannion, France)
    - Nd:YAG laser, 1064 nm, Bernoulli LIBS, laser pulse 10 ns (Litron, Warwickshire, United Kingdom)
- LabTrace 1 (CEITEC, Brno, Czech Republic)
    - Nd:YAG laser, 532 nm, laser pulse 6 ns Litron (UK)
    - Nd:YAG laser, 1064 nm, laser pulse 6 ns Litron (UK)
    - Nd:YAG laser, 266 nm, laser pulse 8 ns, Litron (UK)
    - Nd:YAG laser, 1064 nm, Brilliant (Quantel, Lannion, France)
- AvaSpec EVO-LTG6 (Starline spectrometer, Apeldoorn, Netherlands)
- CMOS detector (Starline, Apeldoorn, Netherlands)
- Shamrock SR-500i spectrometer (Oxford Instruments, Abingdon, United Kingdom)
- iStar 734 ICCD detector (Oxford Instruments, Abingdon, United Kingdom)

4.2.2 Used software

For the measurement of the samples, the following software was used:

- LIBS Navigator (CEITEC, Brno, Czech Republic),
- Litron Control (Litron, Warwickshire, United Kingdom),
- Spectra Controller (Lightigo, Brno, Czech Republic),
- Andor Solis (Oxford Instruments, Abingdon, United Kingdom).

The following software was used for data processing:

- LIBS Analyzer (CEITEC, Brno, Czech Republic),
- MS Office (Microsoft Corporation, Redmond, Washington),
- Origin 2020b (OriginLab, Northampton, USA),
- ImageJ Fiji (National Institute of Health, Bethesda, USA).

4.3 Preparation of samples

First, a calibration set of samples were prepared for different concentrations of Pb (concentration ranging from 100 ppm with a step of 100 ppm up to 1000 ppm) in the sample. A preliminary analysis of this set, led to the conclusion that the best lead concentration for LIBS optimization varies between 300 and 450 ppm. Thus, a concentration of 400 ppm was chosen for the following sample set preparation. The hydroxyapatite standard samples used in this study were prepared by Ing. Lenka Michlovská, Ph.D., who is a part of the research group led by Assoc. Prof. Lucy Vojtová, Ph.D. at CEITEC BUT. The samples were shaped into pellets with a diameter of approximately 5 mm and a thickness of around 1.5 mm. A total of five sets of samples were prepared, as shown in Table 3. Subsequently, the concentration of lead in the samples was confirmed to match the expected concentration. The results indicate only a small deviation from the intended concentrations. The confirmation was done by Mgr. Lucie Šimoníková from MUNI using the ICP-OES method. All five sets of samples had a lead concentration of approximately 390 ppm, and it has been confirmed that the samples were homogeneous. Hydroxyapatite, being the main mineral component of bones, serves as an appropriate representation of bone tissue. This substitution allows for the investigation of heavy metal detection in a bone-like material while overcoming ethical constraints and the challenges associated with acquiring actual bone samples. By using hydroxyapatite samples, this research ensures a valid and representative analysis of heavy metal detection in bone-like materials.

Table 3: Concentration of Pb in hydroxyapatite standards obtained by ICP-OES.

Name of set	Pb (mg/kg)	SD (mg/kg)
Set 1	377	3
Set 2	384	7
Set 3	382	6
Set 4	393	3
Set 5	385	5

4.4 LIBS measurements

In this thesis, three different LIBS systems were utilized. The first system used was the LabTrace 1, which employed single-pulse LIBS and orthogonal double-pulse LIBS. This system is depicted in Figure 14.

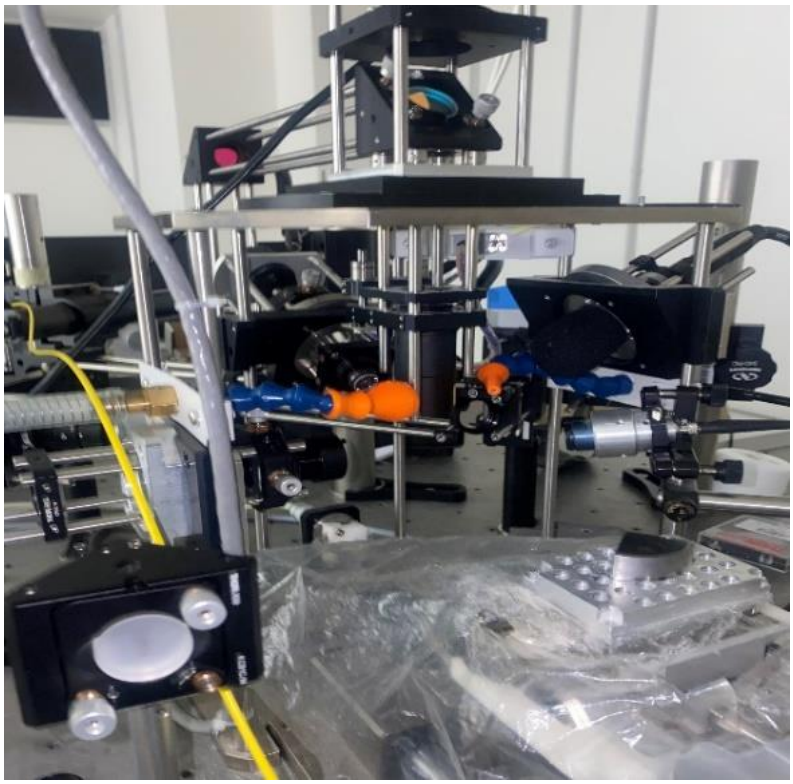

Figure 14: System LIBS LabTrace 1.

Three different lasers were used, with wavelengths of 1064 nm (maximum energy of 200 mJ), 532 nm (maximum energy of 100 mJ), and 266 nm (maximum energy of 10 mJ), respectively. The first two laser wavelengths had a pulse duration of 6 ns, while the third laser had a pulse duration of 8 ns. An optics triplet with a focal distance of f = 35 mm was utilized. Following single-pulse LIBS, the combination of 1064 nm and 532 nm was utilized for orthogonal double-pulse optimization of parameters. A different laser for 1064 nm (Brilliant) was used, and the optics were changed to a singlet with a focal distance of f = 50 mm. The double-pulse had an orthogonal configuration, and the h of the main pulse was 1.5 mm, optimized to avoid sample damage and based on previous laboratory experience. Single-pulse was measured in argon gas purge, while argon was not used in double-pulse measurements, due to its negligible impact on the experimental outcomes. This wavelength combination was the only one used for a double-pulse because it could not be instrumentally achieved with any other combination. However, the combination of 532 nm (maximum energy of 100 mJ) and 1064 nm (maximum energy of 200 mJ) was also performed on a different LIBS system, the Discovery, where a collinear configuration of the double-pulse was possible. Here, both lasers had a pulse duration of 10 ns. Finally, after all optimizations were completed, ablation craters were measured using the FireFly LIBS System. The LIBS system Discovery is depicted in Figure 15.

Figure 15: System LIBS Discovery [45].

To ensure accuracy within the measurement of a single wavelength of laser, it is important that the pulse length remains constant. This is crucial because the pulse length can also affect the intensity of the signal. A longer wavelength can cause greater plasma instability, as during a longer period, there is a greater chance that the energy will not spread uniformly. On the other hand, a longer duration can result in a higher signal intensity.

The same detectors and spectrometers mentioned in Section 4.2.1 were used for all measurements. The Czerny-Turner (Shamrock) spectrometer had a spectrometer slit size of 50 µm, which is tunable, while the Czerny-Turner (Avantes) had a slit width of 25 µm. The sCMOS camera had to be cooled down to 0 °C before every measurement. The gain of the Shamrock was set to 4000 for the experiments conducted in this study.

The specimens were positioned on XYZ motorized stage and the chamber was closed in the case of the Discovery system and sealed in the case of the LabTrace LIBS system. The argon gas flow rate was set to $9\ \mathrm{l} \cdot \mathrm{min}^{-1}$ for single-pulse measurements. The repetition rate was 1 Hz for every measurement.

4.4.1 Optimization of parameters for single-pulse LIBS

In this work, lead was analyzed using spectral line Pb I 405.78 nm. Firstly, measurements were performed for single-pulse LIBS (SP-LIBS). As stated in the theoretical part of the diploma thesis, some of the parameters that affect the signal in measurements are gate delay, defocus, laser energy, and laser wavelength. Single-pulse LIBS measurements were performed with a 5×5 map and in single shot mode, meaning that the signal was not accumulated. The step size was set to 250 µm to avoid crater overlapping, as the measured

crater sizes in single-pulse LIBS averaged around 160µm. Although measurements were performed on both the Shamrock and Avantes spectrometers, data obtained from the Shamrock was more precise for lead analysis because the laser wavelength could be precisely set to measure lead and there was no interference from other spectral lines. For each laser wavelength, five different defocus values were tested in combination with five energies and five gate delays, which means that 125 parameter combinations were tested for one laser wavelength, each resulting in 25 obtained spectra. The only difference was for the 266 nm laser wavelength, where only four energies were tested, with a maximum laser energy of 10mJ, and even with a small measurement step of 1mJ, it was unnecessary to measure energies less than 7mJ because the signal decreased significantly. The discussion of the best parameters is presented in Chapter 5. Tables 4, 5, and 6 present different parameters for different laser wavelengths.

Table 4: Optimization of parameters for 1064 nm laser wavelength.

Laser wavelength (nm)	1064
Energy (mJ)	{60, 50, 40, 30, 20}
Gate delay (µs)	{1, 2, 3, 4, 5}
Defocus (mm)	{0.4, 0.9, 1.4, 1.9, 2.4}

Table 5: Optimization of parameters for 532 nm laser wavelength.

Laser wavelength (nm)	532
Energy (mJ)	{60, 50, 40, 30, 20}
Gate delay (µs)	{0.50, 1.00, 1.25, 1.50,1.75}
Defocus (mm)	{-1.0, -0.5, 0.0, 0.5, 1.0}

Table 6: Optimization of parameters for 266 nm laser wavelength.

Laser wavelength (nm)	266
Energy (mJ)	{10, 9, 8, 7}
Gate delay (µs)	{0.1, 0.3, 0.5, 0.7, 0.9}
Defocus (mm)	{-2.4, -1.9, -1.4, -0.9, -0.4}

4.4.2 Optimization of parameters for double-pulse LIBS

Just as with single-pulse LIBS, three parameters were changed in double-pulse LIBS (DP-LIBS). However, instead of defocus, which is varied in single-pulse LIBS, in this case, it was fixed because the parameter that is much more important in DP-LIBS is interpulse delay (ID). The defocus setting of the instrument was maintained at 0 mm throughout the study as it is considered to be the optimal focus for 532 nm wavelength for accurate and reliable measurements. Both orthogonal pre-ablation configuration and collinear configuration were used. The original plan was to measure all combinations of wavelengths,

but due to instrumental limitations, only the combination of 1064 nm and 532 nm with two different configurations was tested. It is also important to mention that in the orthogonal configuration, there are pre-ablation and reheating configurations. The pre-ablation configuration was used because reheating excites electrons that were not excited with a single-pulse, i.e., they have high energy levels. However, this does not apply to Pb detection, so only pre-ablation was used to ablate in air. The aim of this experiment was to further enhance the LOD obtained from single-pulse LIBS. The aforementioned advice was acquired from the thesis consultants, who based their recommendations on their extensive experience with LIBS, as well as their thorough review of pertinent literature.

In the orthogonal configuration, the first pulse was emitted from a 1064 nm laser. The energy of this pulse was fixed at 180 mJ as no significant difference was observed by varying its energy. However, the energy of the second ablation pulse was varied. In the collinear configuration, the first pulse was emitted from a 532 nm laser, and the energy ratio of 532 nm:1064 nm varied in a 1:2 proportion based on the consultants' recommendations to achieve the most optimal results. Those settings were proven to be optimal in the already published article by Rizwan A. et al. [46]. This decision was supported by already published work on SP-LIBS. Unlike in single-pulse LIBS, 3×3 maps were created in double-pulse LIBS due to larger craters with an average value of about 0.18 mm. Thus, a step size of 500 µm was set to avoid overlapping. Therefore, for each measurement, nine spectra were obtained without accumulation, and a single-shot mode was used. In the orthogonal configuration, we varied five laser energies of 532 nm and used combinations of five gate delays and five interpulse delays, resulting in a total of 125 combinations for this configuration. On the other hand, four energies were tested in the collinear configuration in combination with five interpulse delays and 5 gate delays, resulting in 100 combinations. One of the reasons why higher energies were not used in the collinear configuration, although the system could handle them, was that the AvaSpec spectrometer used for obtaining the spectra became saturated. This saturation was not due to the ICCD detector's saturation but was caused by the chosen Pb emission line being resonant and susceptible to the self-reversed absorption effect, which is particularly pronounced at higher energies. According to NIST, the energy level difference for the Pb I transition that produces a resonant wavelength of 405.78 nm is 1.3205 eV. As explained by the thesis supervisor, resonant emission lines are more prone to a change in plasma density, resulting in a denser plasma and self-reversed absorption. Moreover, higher energy also leads to a higher temperature, resulting in thermal broadening, which can alter the spectral line shapes and cause saturation.

A noticeable difference in the interpulse delay used can be observed between the collinear and orthogonal configurations, with a significantly smaller delay utilized in the former. This can be attributed to the discovery during initial optimization for gate delays that the values employed in the collinear configuration yielded the most optimal signal results.

All parameters for the orthogonal and collinear configurations are presented in Table 7 and Table 8, respectively.

Table 7: Optimization of parameters for orthogonal configuration.

Laser wavelength (nm)	532 + 1064
Energy (mJ) for 532 nm laser	{60, 50, 40, 30, 20}
Energy (mJ) for 1064 nm laser	180
Gate delay (μs)	{1.5, 2.0, 2.5, 3.0, 3.5}
Interpulse delay (μs)	{2, 4, 6, 8}

Table 8: Optimization of parameters for collinear configuration.

Laser wavelength (nm)	532 + 1064
Energy (mJ) for 532 nm laser	{40, 30, 20, 10}
Energy (mJ) for 1064 nm laser	{80, 60, 40, 20}
Gate delay (μs)	{1.0, 1.5, 2.0, 2.5, 3.0}
Interpulse delay (μs)	{0.1, 0.5, 1.0, 1.5, 2.0}

5 Results and discussion

As mentioned in earlier chapters, there are multiple factors that affect the strength of the signal in LIBS analysis. In the theoretical section of this thesis, both SBR and SNR were discussed. However, in this thesis, all graphs are presented using SBR because of better results' visualization.

To calculate SBR using a LIBS Analyzer, the emission line peak and background were manually selected, as shown in Figure 16. By manually selecting the emission line peak and background, it became possible to ascertain the signal intensity and background noise levels. Subsequently, this information was utilized to compute the SBR value. The aim was to achieve the highest possible SBR.

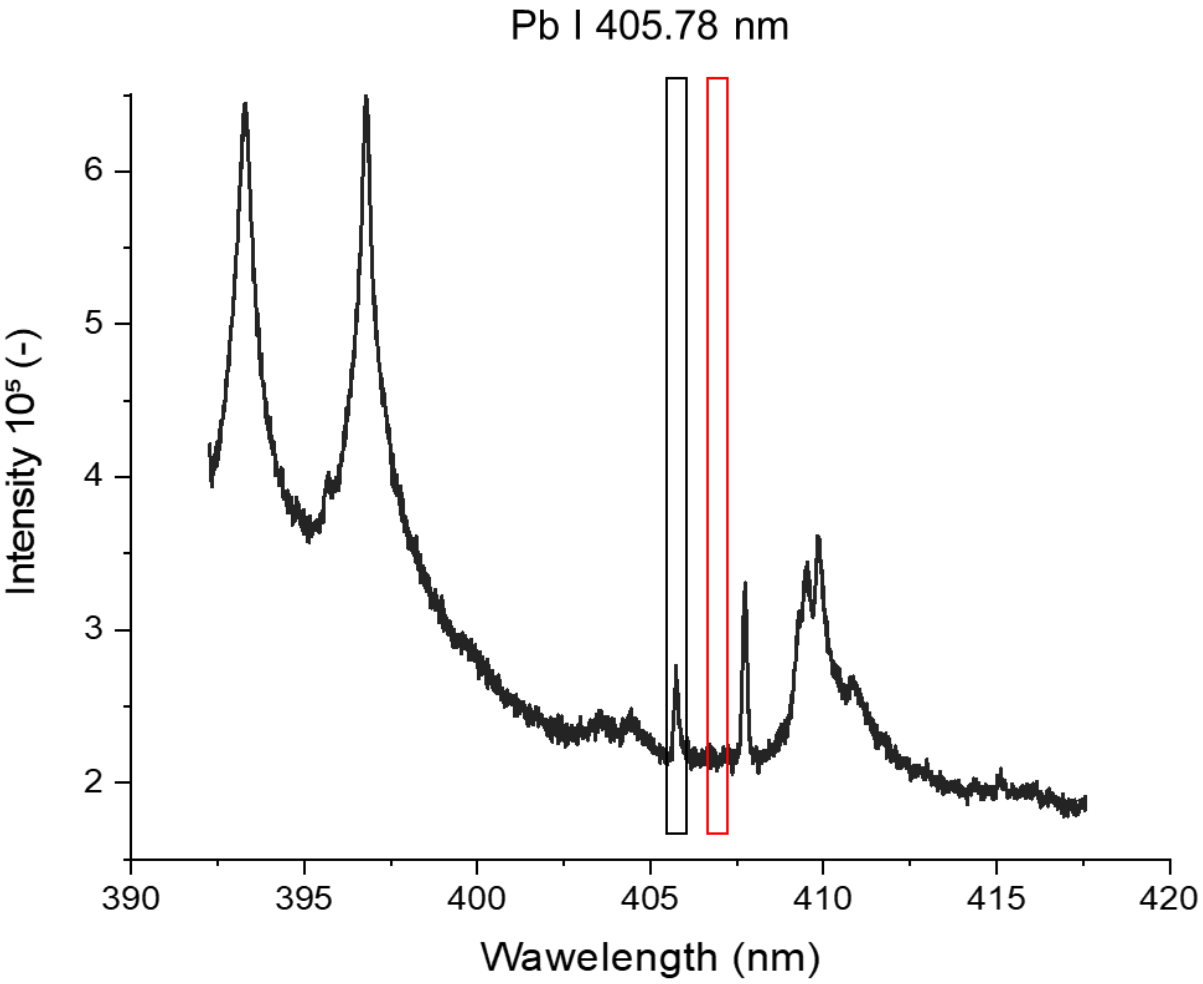

Figure 16: Representation of the selection of the lead emission line and background for the calculation of SBR – Pb line (black), background (red).

The primary focus was on SBR during the selection of optimal parameters for lead analysis in hard tissues. It should be noted that other important parameters include **ablation crater size** and **LOD**.

The calculation of LOD is described in Chapter 2.2.1, and in this study, the formula (3) presented in that chapter was used. This formula is suitable for analyses without calibration

or when the signal is measured for only one known concentration. Although the mentioned formula is commonly used, it has a limitation where the standard deviation (SD) is a point value while $\overline{X_{\mathrm{Pb}}}$ represents the area under the curve, making the units inconsistent. However, this formula has been used in previous studies listed in the references next to the formula and was therefore used in this study. The goal was to achieve the smallest possible LOD, as the aim was to detect very low concentrations of lead in tissues.

The ablation craters' photos were captured using the LIBS FireFly system and analyzed in the ImageJ program. The average ablation crater size was determined by measuring three ablation craters from each parameter setting. They did not show significant variation within a single laser wavelength. The smaller the ablation crater, the higher the resolution.

In single-pulse LIBS, it is important to note that the size of the ablation crater is influenced by the changing parameters of energy and defocus, while gate delay does not affect it. In DP-LIBS, defocus remained constant, and interpulse delay only caused changes in collinear configuration. In the orthogonal configuration, pre-ablation was used, and the first pulse did not affect the crater, nor had the interpulse delay. Craters were measurable in the orthogonal configuration, but not in the collinear configuration, as the high laser energy dispersed the samples and made it impossible to distinguish the craters. The average ablation crater depending on the energy in the orthogonal configuration of DP-LIBS, as well as the average ablation crater for a specific wavelength in single-pulse LIBS, depending on energy and defocus, are presented in Table 9 and Table 10, respectively.

Table 9: Ablation crater dependence on laser energy – double-pulse LIBS.

Energy (mJ) for 532 nm laser – orthogonal configuration	60	50	40	30	20
Ablation crater (mm)	0.167	0.182	0.192	0.178	0.172

As mentioned above, within a single wavelength there is not a significant difference in the size of the ablation crater, but the difference is particularly noticeable between single-pulse and double-pulse LIBS. Crater size is one of the main parameters that has been considered when selecting optimal LIBS parameters.

When analyzing LIBS data, it is common to create dependencies and graphs based on irradiance (I_{e}) rather than energy. This physical quantity is particularly useful because it encompasses both defocus and energy, making graphs, heatmaps, or any other form of data representation more concise.

Table 10: Ablation crater dependence on laser wavelength, defocus, and energy – single-pulse LIBS.

Energy (mJ) for 1064 nm laser	Defocus (mm)	Ablation crater (mm)	Energy (mJ) for 532 nm laser	Defocus (mm)	Ablation crater (mm)	Energy (mJ) for 266 nm laser	Defocus (mm)	Ablation crater (mm)
60	0.4	0.181	60	-1.0	0.188	10	-2.4	0.159
60	0.9	0.168	60	-0.5	0.182	10	-1.9	0.160
60	1.4	0.162	60	0.0	0.183	10	-1.4	0.157
60	1.9	0.172	60	0.5	0.164	10	-.09	0.169
60	2.4	0.176	60	1.0	0.166	10	-.04	0.168
50	0.4	0.171	50	-1.0	0.183	9	-2.4	0.159
50	0.9	0.165	50	-0.5	0.180	9	-1.9	0.165
50	1.4	0.166	50	0.0	0.181	9	-1.4	0.160
50	1.9	0.173	50	0.5	0.162	9	-.09	0.161
50	2.4	0.175	50	1.0	0.168	9	-.04	0.159
40	0.4	0.180	40	-1.0	0.183	8	-2.4	0.155
40	0.9	0.172	40	-0.5	0.182	8	-1.9	0.160
40	1.4	0.169	40	0.0	0.173	8	-1.4	0.157
40	1.9	0.168	40	0.5	0.160	8	-.09	0.161
40	2.4	0.167	40	1.0	0.173	8	-.04	0.164
30	0.4	0.183	30	-1.0	0.185	7	-2.4	0.165
30	0.9	0.183	30	-0.5	0.179	7	-1.9	0.165
30	1.4	0.168	30	0.0	0.181	7	-1.4	0.166
30	1.9	0.169	30	0.5	0.162	7	-.09	0.165
30	2.4	0.178	30	1.0	0.173	7	-.04	0.170
20	0.4	0.181	20	-1.0	0.182			
20	0.9	0.182	20	-0.5	0.177			
20	1.4	0.175	20	0.0	0.179			
20	1.9	0.158	20	0.5	0.164			
20	2.4	0.171	20	1.0	0.168			

Irradiance is calculated as follows:

$$\theta_e = E \cdot t_p, \tag{4}$$

where θ_e (J/s) is radiant flux, E is energy (J), and t_p (s) is pulse length of the laser.

Then, irradiance is defined as:

$$I_e = \frac{\theta_e}{S}, \tag{5}$$

where S (cm^2) is the area of the crater and is defined as:

$$S = \frac{\pi \cdot d^2}{4}, \tag{6}$$

and d (cm) is the diameter of the ablation crater, which is influenced by defocus. The obtained irradiance is then converted to units of GW/cm^2 [47].

In this study, irradiance was calculated only for single-pulse LIBS and orthogonal configuration of double-pulse LIBS, precisely because it was not possible to measure the craters in the collinear configuration of double-pulse LIBS. Thus, for a comparison of both DP-LIBS configurations irradiance was not used. Instead, heatmaps created in Origin were based on energy in order to enhance the visibility of the comparison between the orthogonal and collinear configurations. The next chapter delves into the dependencies of SBR on various adjustable parameters.

The irradiance in LIBS can be indirectly influenced by the depth of defocus. The online tools available at [48–49] were used to calculate the depth of focus (DOF) with the optimal parameters. The walls of craters confine plasmas, affecting their parameters and LIBS analysis results. While shallow craters may increase plasma emission, deeper craters may lead to a decrease in signal due to the shift of collection optics relative to the plasma plume core and different amount of ablated mass, where it decreases with increasing depth of the crater. This becomes particularly crucial when performing depth profiling LIBS analysis [50].

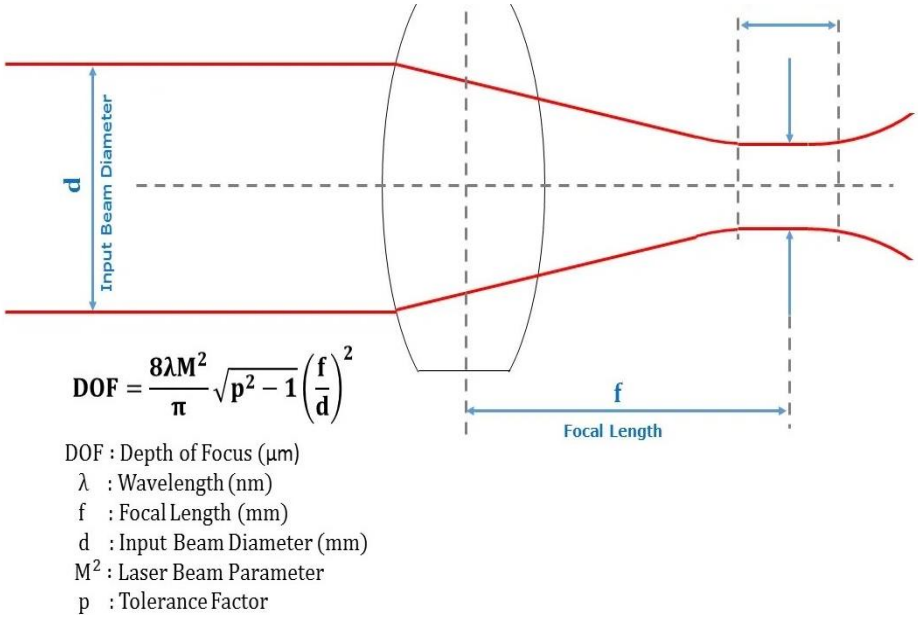

Figure 17: DOF calculation. [48].

The depth of focus (DOF) can be calculated with the given parameters as follows: Laser wavelength of 1064 nm, focal length of 35 mm, input beam diameter of 6.4 mm, tolerance factor of 1.05, and laser beam parameter of 1.9. The resulting DOF is 49.29 μm. DOF calculation is shown in Figure 17.

5.1 Single-pulse (SP) LIBS

5.1.1 266 nm wavelength

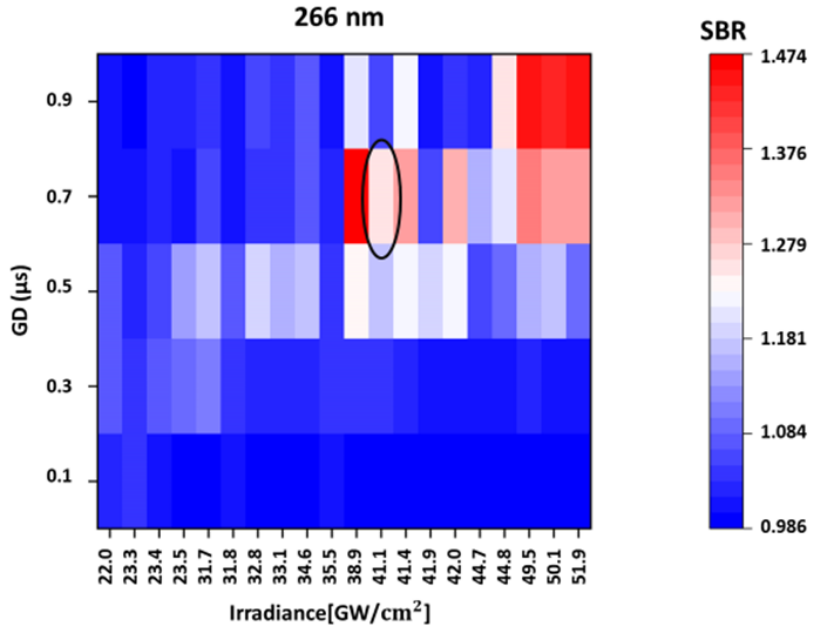

Figure 18: Dependence of SBR on irradiance and GD for 266 nm laser wavelength shown by heatmap.

In the context of measurements for a 266 nm laser, the highest SBR was achieved when using the highest irradiance in combination with the highest gate delay. It is worth noting that the resulting ablation crater did not exhibit significant changes under these parameters at this particular wavelength. Therefore, the ablation crater was not taken into consideration when discussing the optimal parameters for this wavelength. However, the limit of detection was taken into account, and the optimal measurement result was achieved when the gate delay was set to 0.70 μs, and the irradiance was 41.12 GW/cm^2 (with a defocus of -0.9 mm and energy of 9 mJ). At these optimal parameters, the LOD was found to be 226 ppm. The optimal result is also indicated by a black circle in Figure 18. The achieved SBR was 1.26.

5.1.2 532 nm wavelength

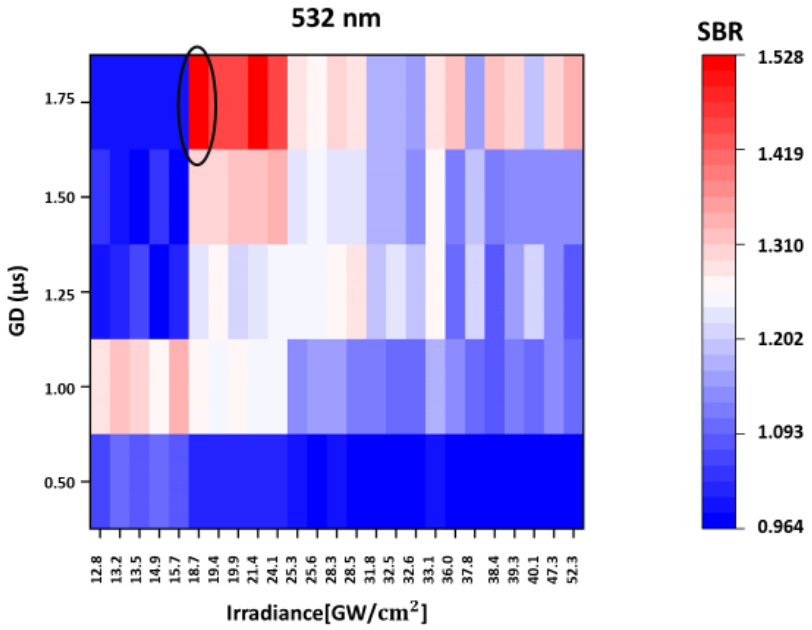

Figure 19: Dependence of SBR on irradiance and GD for 532 nm laser wavelength shown by heatmap.

In the case of using a 532 nm laser for measurements, the best results were obtained when using lower irradiances and higher gate delays. For the optimal measurement, the resulting ablation crater was measured to be 0.17 mm, with an achieved SBR of 1.52. With the LOD taken into account, the optimal measurement result was achieved when the gate delay was set to 1.75 µs, and the irradiance was 18.67 GW/cm^2 (with a defocus of 1 mm and energy of 30 mJ). At these optimal parameters, the LOD was found to be 251 ppm, which represents a significant improvement over other settings for this particular laser wavelength. The optimal result is also highlighted in Figure 19 with a black circle.

5.1.3 1064 nm wavelength

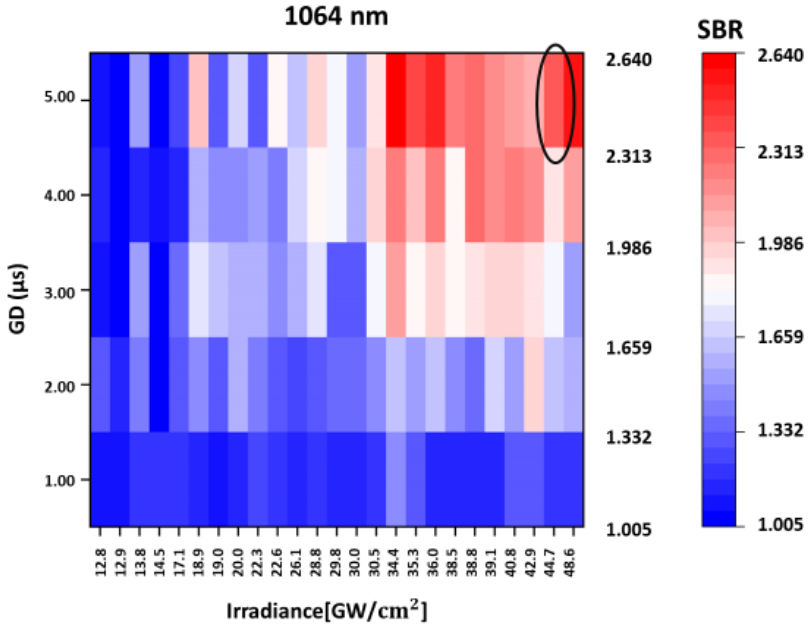

Figure 20: Dependence of SBR on irradiance and GD for 1064 nm laser wavelength shown by heatmap.

In the case of using a 1064 nm laser for measurements, the best results were obtained when using higher gate delays and irradiance. The resulting ablation crater was measured to be 0.16 mm, with an energy of 60 mJ and a defocus of 1.4 mm. The achieved SBR was 2.57, and the LOD was 135. It is worth noting that gate delays had a significant impact on the results, as the signal was markedly lower at gate delays of 1 and 2 µs. The optimal gate delay for the 1064 nm laser was found to be 5 µs, with an irradiance of 48.54 GW/cm^2. These settings resulted in a significant improvement in LOD and overall measurement accuracy. The optimal result is highlighted in Figure 20 with a suitable indicator.

5.2 Double-pulse (DP) LIBS

5.2.1 Orthogonal configuration

Optimal parameters were also determined for the double-pulse orthogonal configuration, which utilized both a 1064 nm pre-ablation pulse and a 532 nm ablation laser pulse. Th resulting ablation crater was measured to be approx. 0.18 mm, demonstrating an increase compared to the single-pulse mode. The optimal energy of the ablating pulse was set to 50 mJ, with an interpulse delay of 2 µs and a gate delay of 3.5 µs. The SBR and LOD were measured to be 2.57 and 181 ppm, respectively. Notably, no visible trend was observed in the results for this configuration. All dependencies are presented in the following Figure 20. The optimal result is marked with a circle in Figure 21.

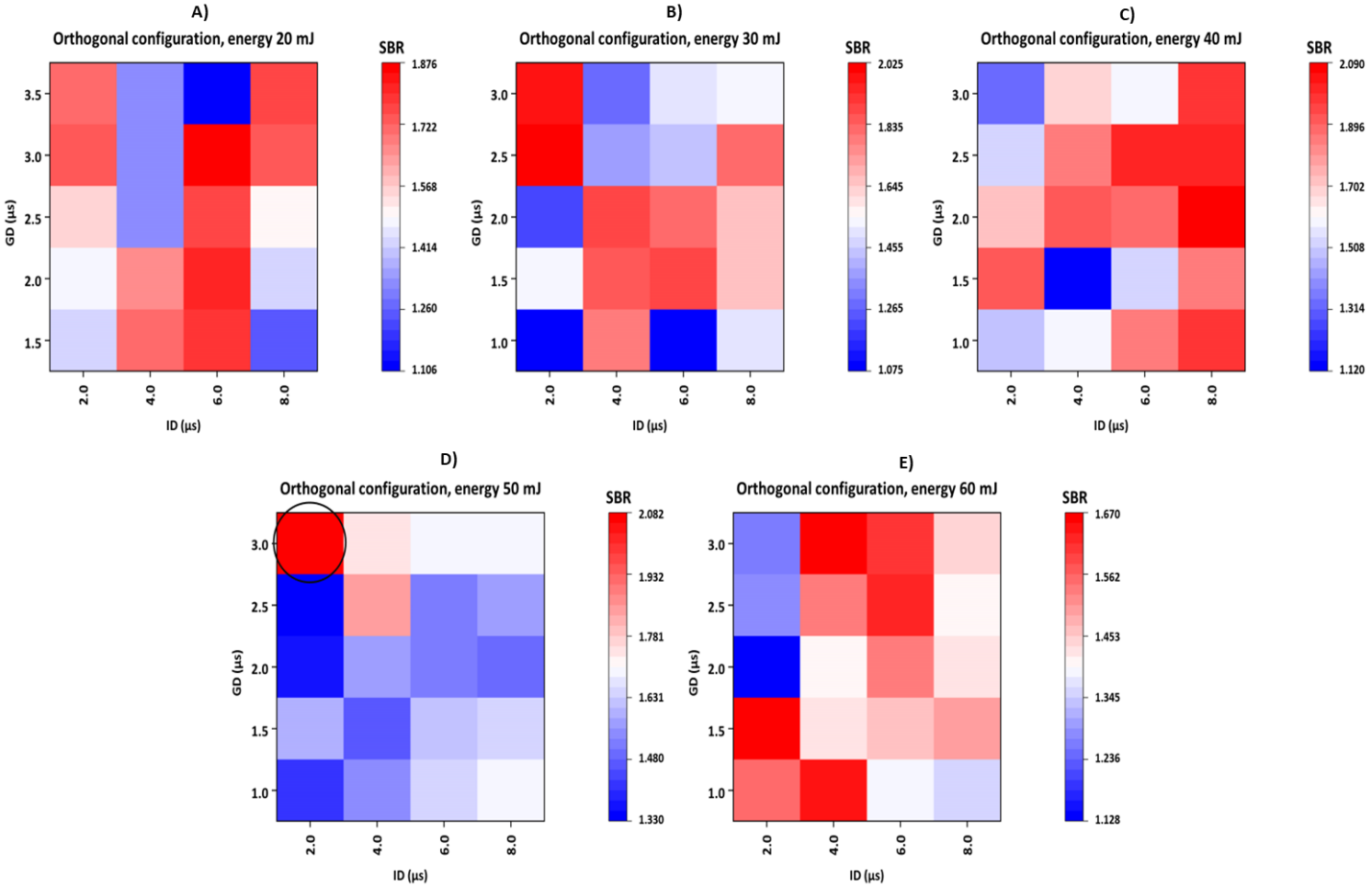

Figure 21: Orthogonal configuration heatmap for SBR dependence on ID, GD and laser energy ((A)20 mJ, B)30 mJ, C)40 mJ, D)50 mJ and E)60 mJ)) – DP-LIBS.

5.2.2 Collinear configuration

The optimal parameters for the double-pulse collinear configuration were again chosen based on the criteria of achieving the lowest LOD and highest SBR values. For the selected optimal parameters, the ablating pulse energy was set to 10 mJ, with an interpulse delay of 2 µs and a gate delay of 3 µs. However, the resulting ablation crater showed significant variation and could not be reliably measured. The SBR and LOD values obtained were 1.75 and 297 ppm, respectively. It was observed that lower energies and higher gate delays tended to produce better signals, while interpulse delay had a relatively minor effect. A comprehensive analysis of these results, along with other important dependencies and trends, can be found in the following Figure 22. The results suggest that for 10 mJ and 20 mJ laser energies, higher SBR can be achieved by using high gate delay in combination with high interpulse delay. However, for laser energies of 30 mJ and 40 mJ, increasing the gate delay led to improved SBR, regardless of the interpulse delay. The optimal result is marked with a circle in Figure 22.

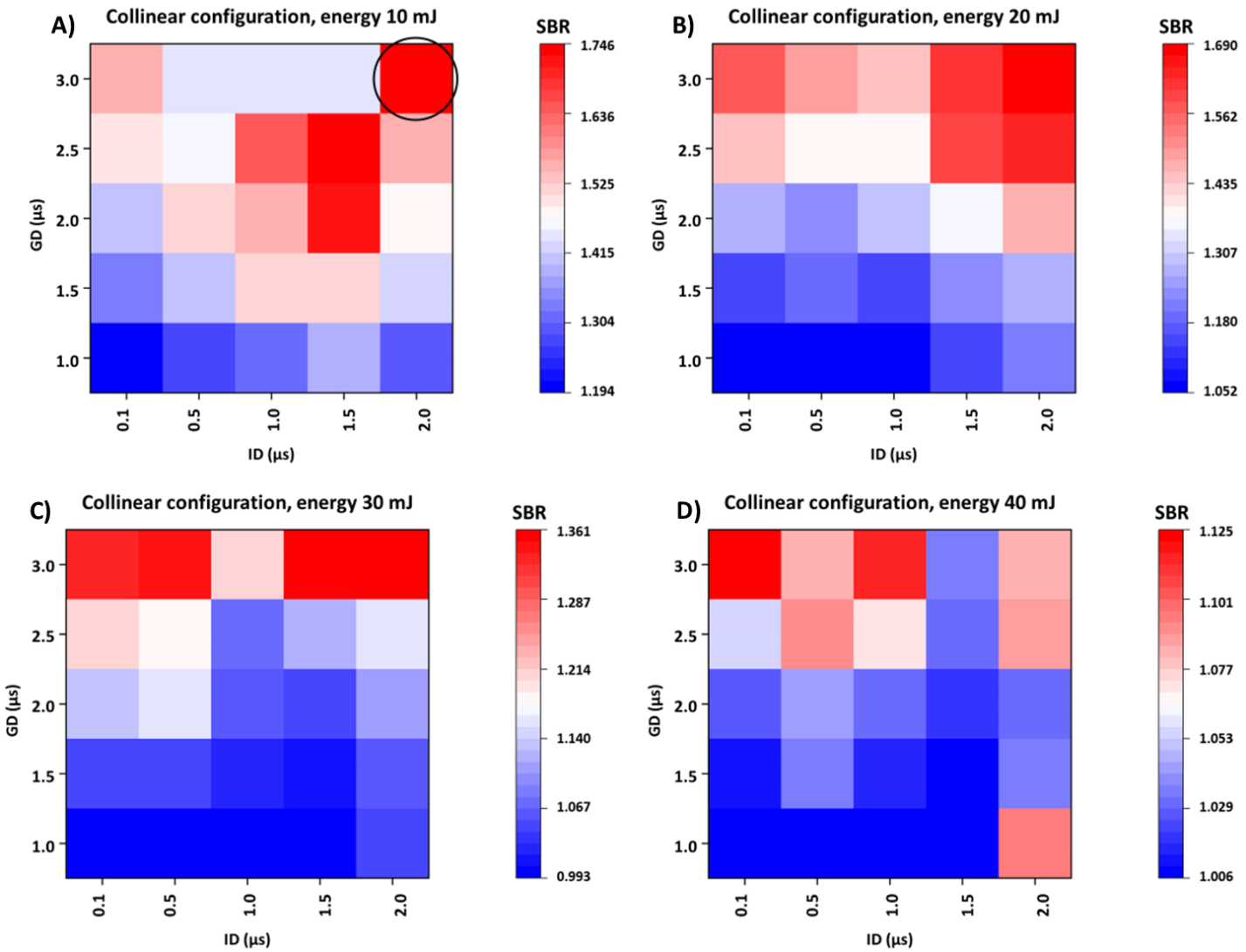

Figure 22: Collinear configuration heatmap for SBR dependence on ID, GD and laser energy (A)10 mJ, B)20 mJ, C)30 mJ, and D)40 mJ) - DP-LIBS.

5.3 Optimal results

Table 11 presents all the optimal parameters selected in the previous sections. It is evident from the table that the single-pulse 1064 nm laser wavelength is the best option, not only because it produces the highest SBR but also because it has the lowest LOD. There could be several reasons why SP outperforms DP. One possible reason for the superiority of SP is that the collection optics we used was not properly set up and angled (at least in the orthogonal configurations where there were no noticeable trends among parameter changes). It is also possible that this is due to the fact that the plasma in double-pulse has more noise and is not as stable as in single-pulse.

Another noteworthy point is that if the entirety of the analyte (Pb) is ablated through single-pulse ablation, there cannot be any further enhancement through double-pulse ablation since there would be no remaining analyte to be ablated.

The table also shows the standard deviations (SD) and relative standard deviations (RSD) of SBR, which play a significant role in determining the quality of the results, such as precision and accuracy.

Table 11: Optimal results for each wavelength and configuration for SP-LIBS and DP-LIBS, as well as highlighting the best possible parameters (blue).

Configuration		**E [mJ]**	**def [mm]**	**GD [µs]**	**spot size [mm]**	**I_e [GW/ cm^2]**	**SBR [-]**	**LOD [ppm]**	**SD [-]**	**RSD [%]**
SP	266 nm	9.00	-0.90	0.70	0.16	41.12	1.26	226.22	0.09	7.3
	532 nm	30.00	1.00	1.75	0.17	18.67	1.52	251.84	0.12	7.7
	1064 nm	60.00	1.40	5.00	0.16	48.54	2.57	135.20	0.30	12.6
DP	Orthogonal	50.00 + 180.00	2.00	3.50	0.18	32.05	2.08	181.20	0.30	14.5
	Collinear	10.00 + 20.00	2.00	3.00	-	-	1.75	297.24	0.19	10.6

The ablation crater produced at the optimal parameters (i.e., energy of 60 mJ and defocus of 1.4 mm) using a 1064 nm laser, is illustrated in Figure 23. Within the image, multiple ablation craters are visible, and the specific one generated at the optimal parameters is denoted by a circle.

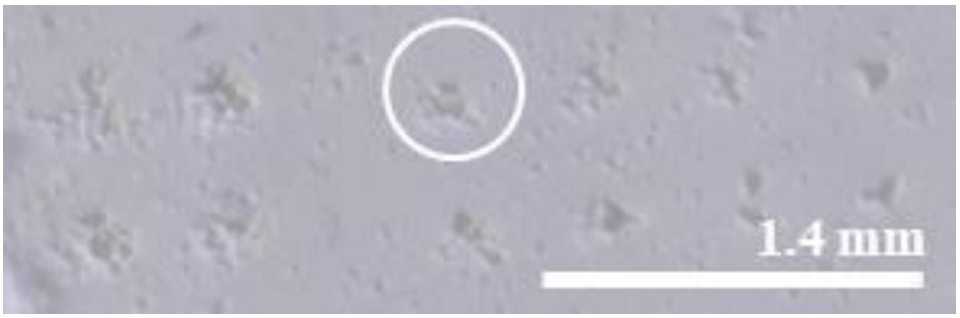

Figure 23: Ablation craters produced by 1064 nm laser wavelength, an energy of 60 mJ, and a defocus of 1.4 mm.

The spectra obtained at the wavelength of 1064 nm and specific energy levels are illustrated in Figure 24, with the 60 mJ energy level highlighted in black. Upon analysis, it was observed that the signal-to-background ratio (SBR) was similar for energy levels of 60 mJ and 50 mJ, whereas the lowest signal was observed at the 20 mJ energy level.

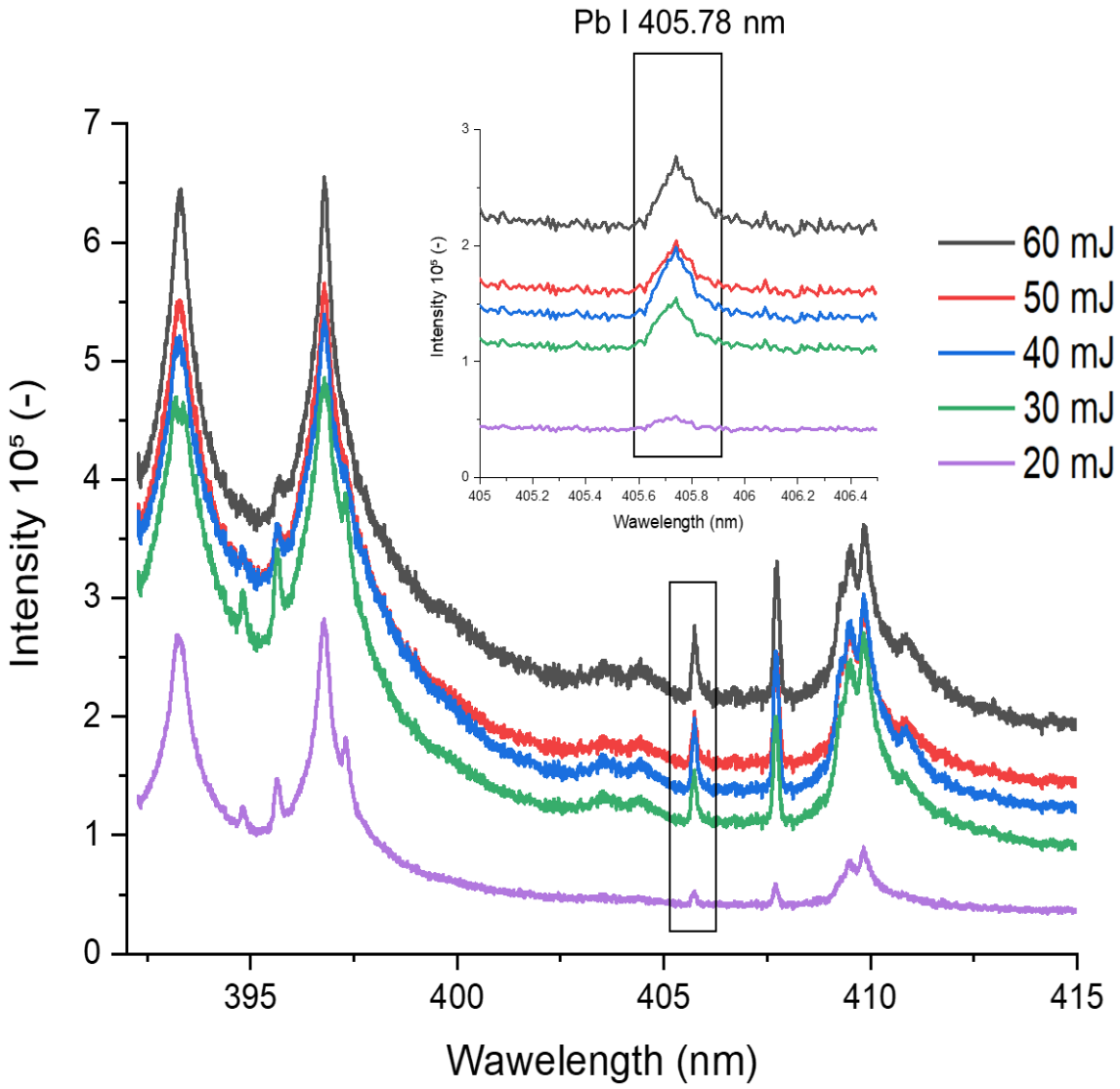

Figure 24: Spectra obtained by 1064 nm laser wavelength. The Pb line is emphasized and magnified in the Figure, but it is important to note that other spectral lines from different elements, including the prominent lines of calcium, are also visible in the spectrum.

The standard deviation of SBR is another critical parameter that was calculated by LIBSAnalyzer for this study. The graphs for all parameter combinations were created by the author of the thesis; however, due to the high number of parameters, only those produced by the 1064 nm laser wavelength, which proved to be the most optimal, are presented in the following Figure 25. The ideal parameters are once again marked by a circle in Figure 26 (A-E). These graphs also demonstrate the dependence of SBR on irradiance, which is an alternate way of presenting the data compared to heatmaps. Each graph depicts a single gate delay, and it is apparent that a larger standard deviation is observed at higher gate delays. However, it is also noticeable that the signal is higher at these delays.

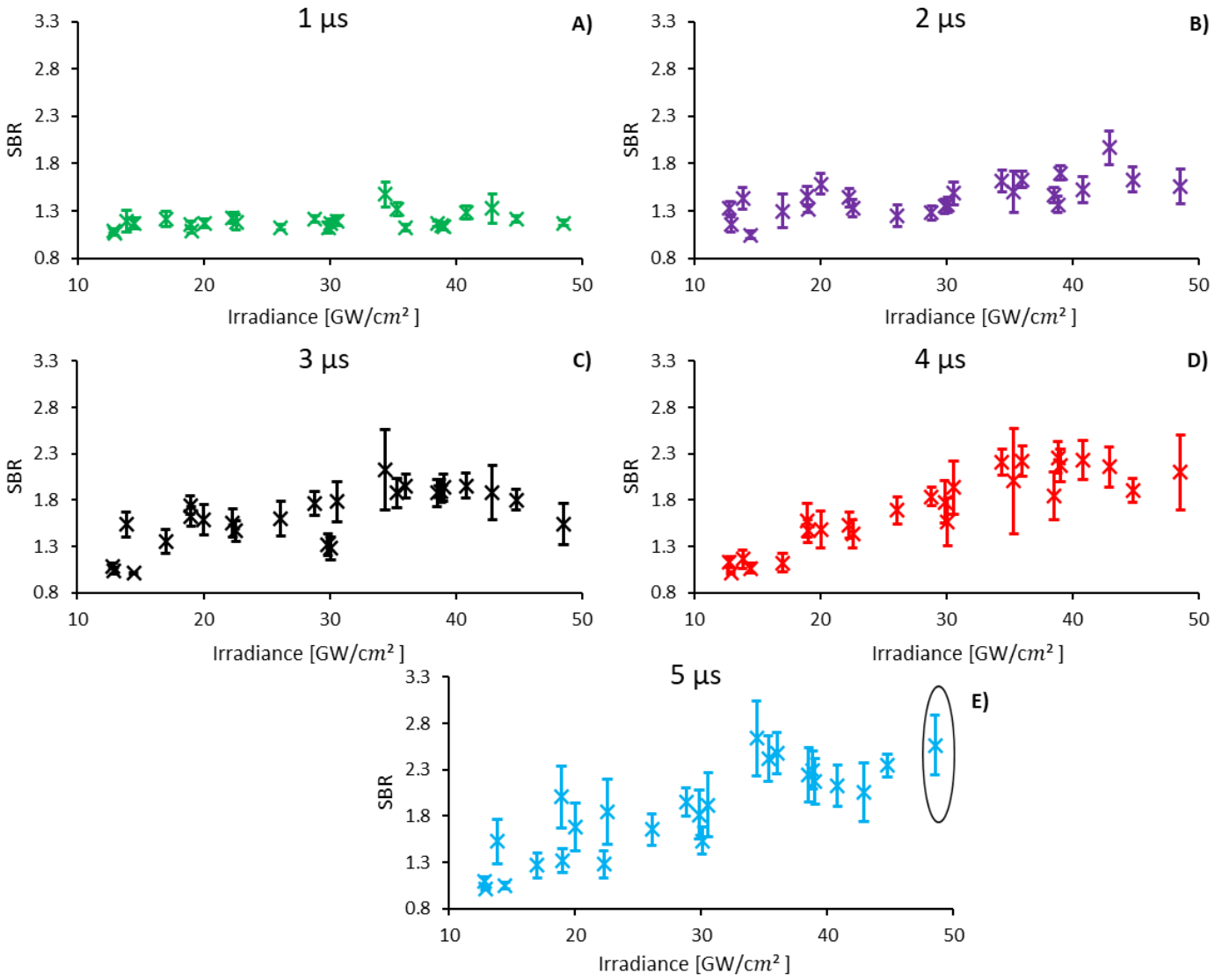

Figure 25: Dependence of SBR on irradiance for different gate delays and 1064 nm laser wavelength for gate delay value: A)1 µs, B)2 µs, C)3 µs, D)4 µs and E)5 µs.

Although the primary objective of this thesis was to measure lead, an AvaSpec spectrometer was also used, which has a wider range and can measure other elements as shown in Figure 26. Given that the focus was on heavy metals, and the observed signal for Pb was weak, these findings are not pertinent to this thesis. Additionally, it is worth noting that the resolution of AvaSpec was inferior to that of Shamrock.

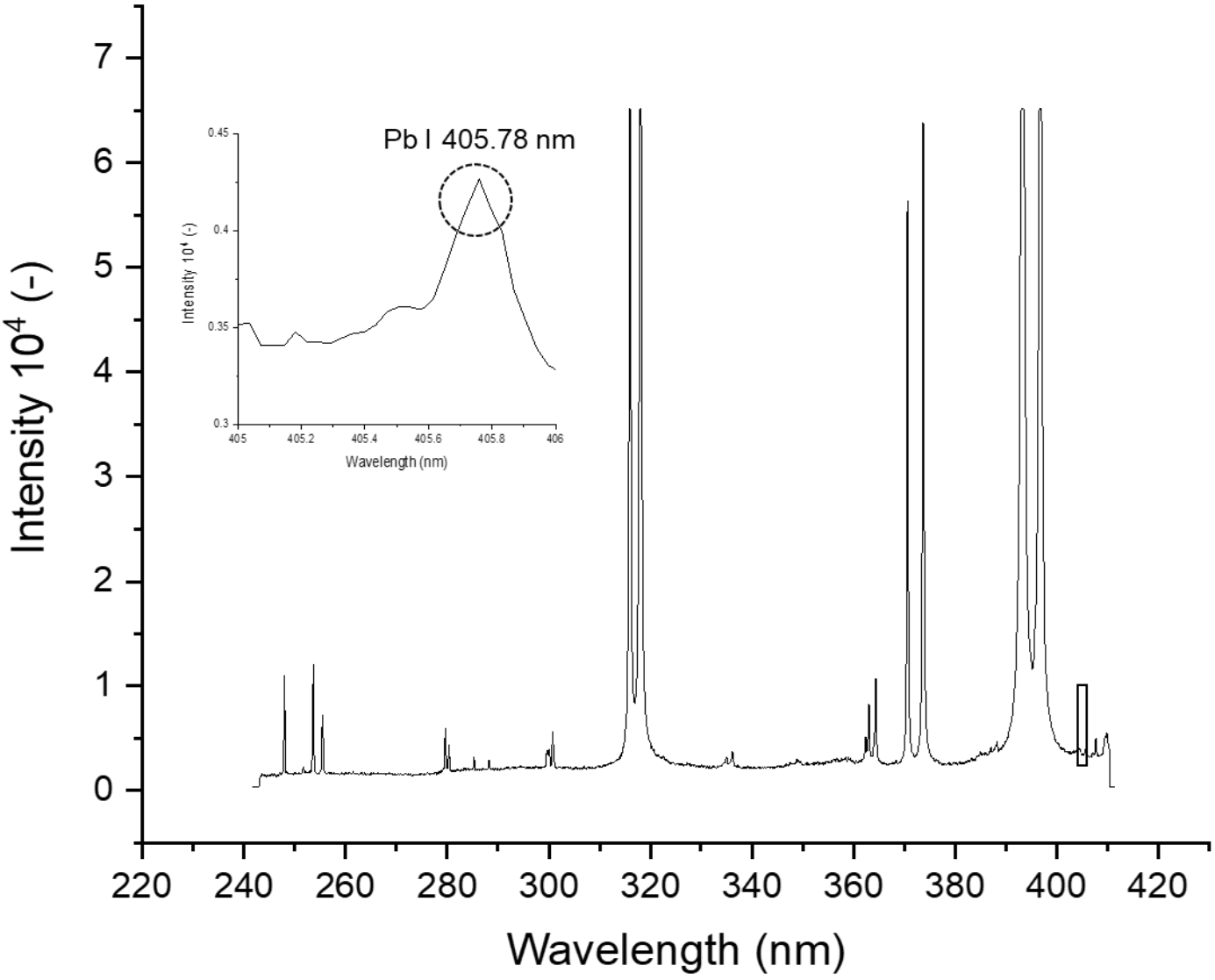

Figure 26: Spectra obtained by 532 nm laser wavelength, and 60 mJ laser energy.

6 Conclusion

This thesis focused on optimizing the parameters for LIBS measurements, with a specific emphasis on the analysis of heavy metals in hard tissues. The importance of spectroscopy in analyzing hard tissues cannot be overstated, as it allows for the early detection of various diseases, including tumor cells. Given the potentially fatal consequences of heavy metal exposure, their detection is of utmost importance. The study primarily analyzed the amount of lead in hydroxyapatite standards as the main sample. Overall, this research provides valuable insights into the optimization of LIBS measurements for the analysis of heavy metals in hard tissues and their potential applications in modern medicine.

The optimized parameters include wavelengths, defocus, energies, gate delays and interpulse delays. Optimized parameters play a crucial role as they not only help in saving time but also contribute to cost reduction in measurements. It is important to note that optimal parameters are primarily required to achieve the best possible results with the highest sensitivity and resolution levels. The main parameters that were considered for optimization were SBR, LOD, and the size of the ablation crater, which directly affects the lateral resolution. By optimizing these parameters, the results can be significantly improved, making LIBS a more reliable and effective technique for analyzing hard tissues.

Three laser wavelengths were tested for SP-LIBS and two configurations for DP-LIBS. On average, approximately 125 different combinations were tested for each wavelength or configuration, resulting in a total of approximately 625 combinations. For each combination, a map was taken, consisting of a 5×5 map for single-pulse and a 3×3 map for double-pulse measurements. This resulted in the collection of 25 measurements for each single-pulse combination and the creation of 25 ablation craters, and nine measurements were taken for double-pulse measurements.

It is possible that the collection optics used in DP-LIBS were not optimally set up and angled, which may have contributed to the superiority of SP-LIBS. Additionally, the instability of the plasma in DP-LIBS and the absence of remaining analyte to be ablated could be factors influencing the performance comparison. When comparing the DP-LIBS configurations, measurable craters were observed in the orthogonal configuration, while the high laser energy dispersed the samples in the collinear configuration, making it challenging to distinguish the craters. However, a noticeable trend was observed in the collinear configuration. In the collinear configuration, it is possible to achieve a higher signal-to-background ratio (SBR) by utilizing a combination of high gate delay and high interpulse delay.

The best results, considering LOD, SBR, and ablation crater, were obtained for a laser wavelength of 1064 nm with an energy of 60 mJ, defocus of 1.4 mm, and gate delay of 1.75 μs. The SBR value was 1.52, LOD was 251.84 ppm, and the ablation crater was approximately 0.17 mm. Thus, this thesis has brought optimized parameters for lead analysis, resulting in improved signal-to-background ratio (SBR), enhanced resolution, and lower limit of detection (LOD). By utilizing these optimized parameters, promising results can be achieved in lead detection, leading to more accurate and reliable outcomes.

In the future, optimal parameters can be further improved by maintaining a high signal-to-background ratio while reducing the ablation crater. This can be achieved by changing the optics and slit width in the spectrometer. Additionally, the LOD can

be improved by using filters that block noise. Real tissues were not used in the measurements due to ethical considerations, limited availability, and the fact that hydroxyapatite, as the main mineral component of bone, represents the structure of real hard tissue well.

Future work in my Ph.D. research will also encompass the analysis of another heavy metal, Cadmium (Cd). By optimizing parameters for the detection and quantification of not just one, but two toxic elements, this research has the potential to make a significant impact in the field of biological studies. The ability to accurately detect and quantify multiple toxic elements will contribute to a better understanding of their effects in biological systems and aid in developing effective mitigation strategies.

7 List of used abbreviations and symbols

LIBS: Laser-induced breakdown spectroscopy

DP-LIBS: Double-pulse LIBS

SBR: Signal-to-background ratio

SNR: Signal-to-noise ratio

Pb: Lead

CF-LIBS: Calibration-free LIBS

ICP-OES: Inductively coupled plasma-optical emission spectrometry

RSD: Relative standard deviation

SD: Standard deviation

ppm: Parts per million

LOD: Limit of detection

LTE: Local thermodynamic equilibrium

fs laser: Femtosecond laser

ns laser: Nanosecond laser

ID: Interpulse delay

GD: Gate delay

CCD: Charge-coupled device

DOF: Depth of focus

8 References

[1] KAKKAR, Rita. *Fundamentals of Spectroscopy. In Atomic and Molecular Spectroscopy: Basic Concepts and Applications*. 2015. Cambridge University Press, 2015. ISBN 9781107479999.

[2] Gamma Scientific. Electromagnetic Spectrum 101: Radio, Microwave and Infrared. In: *Gamma Scientific Inc* [online]. 2021 [cit. 2023-05-07]. Available from: https://gamma-sci.com/2021/07/02/electromagnetic-spectrum-101-radio-microwave-and-infrared/

[3] SAUL, Louise. The Different Types of Spectroscopy for Chemical Analysis. *Azo Optics* [online]. Azo Optics, 2019 [cit. 2023-05-07]. Available from: https://www.azooptics.com/Article.aspx?ArticleID=1382

[4] Spectroscopy: Mastering the Techniques. *Photonics Marketplace* [online]. [cit. 2023-05-07]. Available from: https://www.photonics.com/Articles/Spectroscopy_Mastering_the_Techniques/a25126

[5] HAHN, David and Nicolo OMENETTO. Laser-Induced Breakdown Spectroscopy (LIBS), Part II: Review of Instrumental and Methodological Approaches to Material Analysis and Applications to Different Fields. *Applied Spectroscopy* [online]. 2012, **2012**(66(4), 347-419 [cit. 2023-05-07]. Available from: doi:10.1366/11-06574

[6] What is LIBS?. *Applied Spectra* [online]. Applied Spectra [cit. 2023-05-07]. Available from: https://appliedspectra.com/technology/libs.html

[7] CORSI, Michela, Gabriele CRISTOFORETTI, Montserrat HIDALGO, Daniela IRIARTE, Stefano LEGNAIOLI, Azenio Salvetti SALVETTI and Azenio TOGNONI. Effect of Laser-Induced Crater Depth in Laser-Induced Breakdown Spectroscopy Emission Features. *Applied Spectroscopy* [online]. 2005, **2005**(59(7), 853-860 [cit. 2023-05-07]. Available from: doi:10.1366/0003702054411607

[8] TOGNONI, Elisabetta, Gabriele CRISTOFORETTI, Stefano LEGNAIOLI and Vincenzo PALLESCHI. Calibration-Free Laser-Induced Breakdown Spectroscopy: State of the art. *Spectrochimica Acta Part B: Atomic Spectroscopy* [online]. 2020, **2020**(65), 1-14 [cit. 2023-05-08]. Available from: doi:doi.org/10.1016/j.sab.2009.11.006

[9] BALI, Tibor. *LIBS Spectroscopy and Applications* [online]. 2012 [cit. 2023-05-07]. Available from: https://www.semanticscholar.org/paper/LIBS-spektroskopija-i-primjene-Bali/63b237dacc25240565059eae281d20f03d5aa029

[10] POŘÍZKA, Pavel and Jozef KAISER. *Laser-Induced Breakdown Spectroscopy: Theory and Applications*. [152] Brno, 2022. Available from: https://moodle.vut.cz/pluginfile.php/513401/mod_resource/content/1/LaserSpec_theorapp_2022.pdf

[11] PALLESCHI, Vincenzo, Andrzej W. MIZIOLEK and Israel SCHECHTER. *Laser Induced Breakdown Spectroscopy*. 2006. Cambridge University Press, 2009. ISBN 0521852749.

[12] CRISTOFORETTI, Gabriele, Alessandro GIACOMO, Marcella DELL'AGLIO, Stefano LEGNAIOLI, Elisabetta TOGNONI, Vincenzo PALLESCHI and Nicolo' O OMENETTO. Local Thermodynamic Equilibrium in Laser-Induced Breakdown Spectroscopy: Beyond the McWhirter criterion. *Spectrochimica Acta Part B: Atomic Spectroscopy* [online]. 2010, **2010**(65(1), 86-95 [cit. 2023-05-07]. Available from: doi:10.1016/j.sab.2009.11.005

[13] GHAZEL, Amal, Mohammed TAYEB MEFTAH, Saïd DOUIS and K. CHENINI. Spectral line broadening by electron collisions in plasmas. *Revista Mexicana de Fisica* [online]. 2017, **2017**, 481-485 [cit. 2023-05-07]. Available from: https://www.researchgate.net/publication/319043958_Spectral_line_broadening_by_electron_collisions_in_plasmas

[14] GORNUSHKIN, Igor, Clara M., Benjamin SMITH, James WINEFORDNER, Ulrcih PANNE and Reinhard NIESSNER. Time-resolved resonance shadow imaging of laser-produced lead and tin plasmas. *Spectrochimica Acta Part B: Atomic Spectroscopy* [online]. 1997, **1997**(52(11), 1617-1625 [cit. 2023-05-07]. Available from: doi:10.1016/S0584-8547(97)00062-1

[15] LEI, Wenqi. *Temporal and spatial characteristics of laser-induced plasma on organic materials and quantitative analysis of the contained inorganic elements*. Shanghai, 2012. Université Claude Bernard - Lyon I. Available from: https://www.researchgate.net/figure/Typical-temporal-evolution-of-the-plasma-emission-and-optimal-gating-of-the-detector-for_fig3_278644890

[16] MOROS, Javier and Javier LASERNA. Laser-Induced Breakdown Spectroscopy (LIBS) of Organic Compounds: A Review. *Applied Spectroscopy* [online]. 2019, **2019**(73(9), 963-1011 [cit. 2023-05-07]. Available from: doi:10.1177/0003702819853252

[17] *National Institute of Standards and Technology* [online]. Gaithersburg, Maryland, SAD [cit. 2023-05-20]. Available from: https://physics.nist.gov/PhysRefData/Handbook/Tables/leadtable2.htm

[18] MUSAZZI, Sergio and Umberto PERINI. *Laser-Induced Breakdown Spectroscopy: Theory and Applications* [online]. 2014 [cit. 2023-05-07]. ISBN 978-3-642-45084-6.

[19] SINGH, Jagdish and Surya THAKUR. *Laser-Induced Breakdown Spectroscopy*. 2007. Elsevier Science, 2007. ISBN 978-0-12-818829-3.21PASCHOTTA, Rüdiger. Frequency Doubling. In: *RP Photonics Encyclopedia* [online]. [cit. 2023-05-07]. Available from: https://www.rp-photonics.com/frequency_doubling.html

[20] ESELLER, Kemal and Fang-Yu YUEH. Non-intrusive, on-line, simultaneous multi-species impurity monitoring in hydrogen using LIBS. *Applied Physics B* [online]. 2011, **2011**(102), 963-969 [cit. 2023-05-09]. Available from: doi:10.1007/s00340-010-4202-8.

[21] MANGASI MARPAUNG, Alion, Edward HAREFA, Marincan PARDEDE, et al. Simple defocus laser irradiation to suppress self-absorption in laser-induced breakdown spectroscopy. *Heliyon* [online]. **2022**(8(8), e10057) [cit. 2023-05-07]. Available from: doi:10.1016/j.heliyon.2022.e10057

[22] GIAKOUMAKI, Anastasia, Kristalia MELESSANAKI and Demetrios ANGLOS. Laser-induced breakdown spectroscopy (LIBS) in archaeological science—applications and prospects. *Analytical and Bioanalytical Chemistry* [online]. **2007**(387), 749–760 [cit. 2023-05-07]. Available from: https://link.springer.com/article/10.1007/s00216-006-0908-1

[23] SALEH, Bahaa and Malvin Carl TEICH. *Fundamentals of photonics*. 1. New York: WILEY, 1991. ISBN 9780471839651.

[24] PASCHOTTA, Rüdiger. Q-switches. In: *RP Photonics Encyclopedia* [online]. [cit. 2023-05-07]. Available from: https://www.rp-photonics.com/monochromators.html

[25] PASCHOTTA, Rüdiger Q-switched lasers. In: *RP Photonics Encyclopedia* [online]. [cit. 2023-05-07]. Available from: https://www.rp-photonics.com/q_switched_lasers.html

[26] PASCHOTTA, Rüdiger. Monochromators. In: *RP Photonics Encyclopedia* [online]. [cit. 2023-05-07]. Available from: https://www.rp-photonics.com/monochromators.html

[27] FU, Xinglan, Guanglin LI and Daming DONG. Improving the Detection Sensitivity for Laser-Induced Breakdown Spectroscopy: A Review. *Frontiers in Physics* [online]. 2020, (8) [cit. 2023-05-07]. Available from: doi:10.3389/fphy.2020.00068

[28] PROCHAZKA, David, Prochazka POŘÍZKA, Jan NOVOTNÝ,, Aleš HRDLIČKA, Karel NOVOTNÝ, Petr ŠPERKAB and Jozef KAISER. Triple-pulse LIBS: laser-induced breakdown spectroscopy signal enhancement by combination of pre-ablation and re-heating laser pulses. *Journal of Analytical Atomic Spectrometry* [online]. 2020, **2020**(35(2), 247-256 [cit. 2023-05-07]. Available from: doi:10.1039/C9JA00323A

[29] A. CREMERS, David and Leon J. RADZIEMSKI. *Handbook of Laser-Induced Breakdown Spectroscopy*. West Sussex, England: John Wiley, 2006. ISBN 0470092998, 9780470092996, 9780470093009.

[30] ZHANG, Tianlong, Hongsheng TANG and Hua LI. Chemometrics in laser-induced breakdown spectroscopy: Progress of Chemometrics in Laser-induced Breakdown Spectroscopy. *Journal of Chemometrics* [online]. 2018, **2018**(32) [cit. 2023-05-08]. Available from: doi:10.1002/cem.2983

[31] LIMBECK, Andreas, Lukas BRUNNBAUER, Hans LOHNINGER, et al. Methodology and applications of elemental mapping by laser induced breakdown spectroscopy. *Analytica Chimica Acta* [online]. 2021, **2021**(1147), 72-98 [cit. 2023-05-07]. Available from: doi:https://doi.org/10.1016/j.aca.2020.12.054

[32] JASSIM MOHAMMED AL TIMIMI, Zahra and Mohammed SALEEM ISMAIL ALHABEEL. Laser Dental Treatment Techniques. *Prevention, Detection and Management of Oral Cancer* [online]. 2018, **2018** [cit. 2023-05-07]. ISSN 978-1-78984-503-7. Available from: doi:10.5772/intechopen.80029

[33] KOVAČIĆ, Nataša and Ivan KREŠIMIR LUKIĆ. *Anatomy and Physiology*. 2015. Zagreb: Medicinska naklada, 2015. ISBN 978-953-176-274-8.

[34] FU, Zeyu, Yu ZHUANG, Jinjie CUI, et al. Development and challenges of cells- and materials-based tooth regeneration. *Engineered Regeneration* [online]. 2022, **2022**(3(2), 163-181 [cit. 2023-05-07]. Available from: doi:10.1016/j.engreg.2022.04.003

[35] DAGDEVIREN, Didem, Zana KALAJZIC, Douglas J ADAMS, Ivo KALAJZIC, Alan LURIE, Maija MEDNIEKS and Arthur R HAND. Responses to spaceflight of mouse mandibular bone and teeth. *Archives of Oral Biology* [online]. 2018, 2018, (93), 163-176 [cit. 2023-05-07]. Available from: doi:10.1016/j.archoralbio.2018.06.008

[36] GLAVAŠEVIĆ, Arbutina. *Heavy metals in the body* [online]. Osijek, 2020 [cit. 2023-05-07]. Available from: https://repozitorij.kemija.unios.hr/islandora/object/kemos:398. Josip Juraj Strossmayer University of Osijek.

[37] SINGH, Reena, Neetu GAUTAM, Anurag MISHRA and Rajiv GUPTA. Heavy metals and living systems: An overview. *Indian Journal of Pharmacology* [online]. 2011, **2011**(43(3), 246–253 [cit. 2023-05-07]. Available from: doi:10.4103/0253-7613.81505

[38] SIKIRICA, Milan. *Chemistry 1 - Textbook for the first grade of high school*. 2010. Sarajevo: Sarajevo Publishing, 9958-21-042-6. ISBN 9958-21-042-6.

[39] WINNAND, Philipp, Mark OOMS, Marius HEITZER, Matthias LAMMERT, Frank HÖLZLE and Ali MODABBER. Real-time detection of bone-invasive oral cancer with laser-induced breakdown spectroscopy: A proof-of-principle study. *Oral Oncology* [online]. 2023, **2023**(138) [cit. 2023-05-07]. Available from: doi:https://doi.org/10.1016/j.oraloncology.2023.106308

[40] MARÍN-ROLDÁN, Alicia, Shamaila MANZOOR, Jaroslav KRIŠTOF and Pavel VEIS. Enlarged spectral range in Calibration Free - Laser Induced Breakdown Spectroscopy for the qualitative and quantitative analysis of a complex bone matrix. *Spectrochimica Acta Part B: Atomic Spectroscopy* [online]. 2019, **2019**(156), 13-19 [cit. 2023-05-07]. Available from: doi:10.1016/j.sab.2019.04.005

[41] SAMEK, Ota, David BEDDOWS, Helmut TELLE, Gareth W. MORRIS, Miroslav LÍŠKA and Jozef KAISER. Quantitative analysis of trace metal accumulation in teeth using laser-induced breakdown spectroscopy. *Applied Physics A* [online]. 1999, **1999**(69), 179-182 [cit. 2023-05-07]. Available from: doi:10.1007/s003399900277

[42] J. NASER, Hawraa and Tagreed K. HAMAD. Quantitative Analysis of heavy metals in gallstone Using LIBS. *Journal of Physics: Conference Series* [online]. 2021, **2021**(1963, 012089) [cit. 2023-05-07]. Available from: doi:10.1088/1742-6596/1963/1/012089

[43] LI, Honglian, Chenxing ZHANG, Chun WANG, Shizhao ZHANG, Shijie FU and Lide FANG. RESEARCH ARTICLE| DECEMBER 22 2022 Quantitative analysis of heavy metals by laser-induced breakdown spectroscopy technique in association with temperature control and KCl additive. *Journal of Laser Applications* [online]. 2023, **2023**(35(1), 012007) [cit. 2023-05-07]. Available from: doi:10.2351/7.0000901

[44] KASEM, Mohamed A., Jhanis J GONZÁLEZ, Richard E. RUSSO and Mohamed ABDEL-HARITH. Effect of the wavelength on laser induced breakdown spectrometric analysis of archaeological bone. *Spectrochimica Acta Part B: Atomic Spectroscopy* [online]. 2014, 2014, **2014**(101), 26-31 [cit. 2023-05-07]. Available from: doi:10.1016/j.sab.2014.07.010

[45] Equipment. *Laboratory of Laser Spectroscopy* [online]. 2023: Central European Institute of Technology, 2023, 2023 [cit. 2023-05-19]. Available from: https://libs.ceitec.cz/equipment/

[46] RIZWAN, Ahmed, Iqbal JAVED and Baig ASLAM. Effects of laser wavelengths and pulse energy ratio on the emission enhancement in dual pulse LIBS. *Laser Physics* [online]. 2015, **2015**(12) [cit. 2023-05-09]. Available from: doi:10.1088/1612-2011/12/6/066102

[47] *What is Fluence?* [online]. Fyshwick Canberra: Australia Scientific Instruments [cit. 2023-05-19]. Available from: https://asi-pl.com.au/what-is-fluence/

[48] *Depth of Focus Calculator* [online]. Wavelength Opto-Electronic (S) [cit. 2023-05-07]. Available from: https://wavelength-oe.com/cs/optical-calculators/depth-of-focus/

[49] Spot size and depth of defocus [online]. Control Laser Corporation, 2021 [cit. 2023-05-14]. Available from: https://www.controllaser.com/services/buyers-guide/spot-size-and-depth-of-focus-calculator/

[50] REHSE, Steven. Biomedical Applications of LIBS. In: *Laser-Induced Breakdown Spectroscopy* [online]. 182. Berlin: Springer, 2014, s. 457-488 [cit. 2023-05-07]. ISBN 978-3-642-45085-3. Available from: https://ui.adsabs.harvard.edu/abs/2014libs.book..457R/abstract